scientific reports

Check for updates

OPEN

Structural analysis and antimicrobial assessment of bioinspired silver nanoparticles from *Ferula communis*

Yasmeen M. G. Alshamari[1,2], Hamad Z. Alkhathlan[3]✉, Ponmurugan Karuppiah[4], Mujeeb Khan[3], Ekram Y. Danish[1], Ahmad Aqel[3], Syed Farooq Adil[3], Mohammed Rafi Shaik[3] & Merajuddin Khan[3]✉

The green synthesis of nanoparticles using plant extracts has garnered significant interest from scientists worldwide due to its advantages over traditional chemical processes. This method is rapid, eco-friendly, non-toxic, and cost-effective. The current study focuses on preparing silver nanoparticles (AgNPs) using *Ferula communis* extract as a green reducing agent. During the study, various parameters were evaluated to study their effect on the shape, size, and yield of the AgNPs. The synthesized AgNPs were thoroughly characterized using multiple techniques, confirming the production of crystalline, spherical-shaped NPs, while the plant extract served as the reducing agent. GC-MS analysis was performed to identify the key phytochemicals responsible for reducing silver salts, as well as to characterize the entire phytochemical spectrum present in the *F. communis* extract. This analysis revealed a total of 67 compounds, with stigmasterol, pentadecanoic acid, (5*E*, 9*Z*)-farnesyl acetone, and pentyl decanoates being the most predominant, possibly playing crucial roles in the synthesis of AgNPs. Furthermore, the antimicrobial activity of the AgNPs against various bacterial and fungal strains was investigated. The results showed that *Staphylococcus aureus* exhibited the largest inhibition zone (10.05 ± 0.05 mm), followed by *Escherichia coli* (9.25 ± 0.05 mm), *Candida albicans* (8.70 ± 0.05 mm), *Pseudomonas aeruginosa* (8.50 ± 0.20 mm), *Aspergillus niger* (8.45 ± 0.00 mm), *Klebsiella pneumoniae* (8.15 ± 0.50 mm), and *Bacillus subtilis* (7.55 ± 0.20 mm). The plant extract was also tested against the same microbial pathogens; however, it only displayed an inhibitory effect against *E. coli*, with an inhibition zone of 6.50 ± 0.10 mm. These results indicate that the synergistic effect between AgNPs and the residual phytoconstituents on the surface of the NPs plays a significant role in enhancing the antimicrobial properties of the resulting material.

Keywords Green synthesis, Silver nanoparticles, Ferula communis, Antimicrobial activity, Biomedical applications

Green nanotechnology is currently a significant area of focus, aiming to facilitate the production of nanotechnology-based products that are eco-friendly and safe for all living beings, while also ensuring sustainable commercial viability[1]. One key aspect receiving considerable attention is the "green synthesis" of metal nanoparticles, which exhibit unique optical, chemical, photochemical, and electronic properties[2]. Metal nanoparticles, particularly noble metals, have been extensively studied due to their strong optical absorption in the visible spectrum, which is a result of the collective excitation of free electrons[3]. Silver nanoparticles (AgNPs) are a notable area of interest among noble metal nanoparticles due to their diverse applications. These applications include nonlinear optics, spectrally selective coatings for solar energy absorption, biolabeling, intercalation materials for electrical batteries, optical receptors, catalysts in chemical reactions[4]. Interest in AgNPs has grown recently due to their antimicrobial properties, which result from their high surface-to-volume ratio and unique physical and chemical characteristics that differ from those of bulk materials[5]. Generally, the antibacterial

[1]Department of Chemistry, Faculty of Science, King Abdulaziz University, P.O Box 80200, Jeddah 21589, Saudi Arabia. [2]Department of Chemistry, College of Science, University of Hail, P.O. Box 2440, Hail 81451, Saudi Arabia. [3]Department of Chemistry, College of Science, King Saud University, P.O. Box 2455, Riyadh 11451, Saudi Arabia. [4]Department of Botany and Microbiology, College of Science, King Saud University, P.O. Box 2455, Riyadh 11451, Saudi Arabia. ✉email: khathlan@ksu.edu.sa; mkhan3@ksu.edu.sa

activity of AgNPs is primarily determined by their surface area and their ability to effectively release silver ions. The large surface area of NPs enhances their contact with microorganisms, allowing them to easily attach to cell membranes and penetrate bacterial cells[6]. The release of ionic silver leads to the inactivation of essential bacterial enzymes, inhibition of DNA replication, and damage to bacterial cytoplasmic membranes, ultimately resulting in cell death[7]. AgNPs can be synthesized using various physical, chemical, and biological methods. However, most commonly used techniques involve toxic chemicals, hazardous conditions, and expensive equipment[8]. In contrast, green synthetic approaches are an advancement over traditional chemical and physical methods. They are cost-effective, environmentally friendly, and easily scalable for large-scale production[9]. These methods do not require high pressure, excessive energy, high temperatures, or toxic chemicals. The green synthesis of AgNPs involves the use of biocompatible ingredients under physiological conditions of temperature and pressure. Additionally, the biologically active molecules that are part of this green synthesis process act as functionalizing ligands, enhancing the suitability of these NPs for biomedical applications[10]. To date, a variety of biocompatible materials have been used to prepare metallic NPs, including AgNPs[11]. These materials encompass microorganisms, marine organisms, microfluids, and plant extracts. Among these, plant extracts are particularly significant as bioreductants. They are relatively easy to handle, readily available, low-cost, and have been extensively studied for the green synthesis of other nanomaterials[12].

The biomolecules in plants including flavonoids, phenolics, steroids, etc., facilitate the reduction of Ag^+ ions from silver nitrate to form AgNPs. This reduction process occurs extracellularly and quickly, resulting in a simple biosynthesis of nanomaterials[13]. The use of plant materials for synthesizing nanomaterials was first reported by Gardea-Torresdey et al.[14]. Following this, extensive research was conducted on the bioreduction of various metals to create nanoscale materials in different shapes, suitable for a wide range of applications. For example, Nadagouda et al. reported the preparation of polydisperse spherical AgNPs with sizes ranging from 5 to 100 nanometers, synthesized using aqueous extracts from coffee and tea leaves[15]. In our recent study, we demonstrated the preparation of spherical AgNPs approximately 20 nanometers in size, using extracts from the aerial parts of the *Anthemis pseudocotula* Boiss, plant. This extract served a dual purpose as both a reducing and stabilizing agent[16]. Similarly, in this study, water extract of *Ferula communis* was used as a green reducing agent.

F. communis, commonly known as giant fennel and belonging to the *Apiaceae* family, is widely used in traditional medicine to treat various ailments, including headaches, hysteria, dysentery, arthritis, and rheumatism[17]. This plant also has antiseptic and antihysteric properties and can serve as an analgesic, depilatory, and diuretic[18]. Furthermore, numerous studies have shown that the root of *F. communis*, referred to as Al-Kalakh in Saudi Arabia, is effective in treating skin infections and stomach disorders[19]. Research indicates that isolated compounds from *F. communis* are rich in bioactive properties, such as anticoagulant[20], antioxidant[21], anticancer[22], and antibacterial activities[23]. The therapeutic effects of this plant can be attributed to a wide range of phytochemicals that act as bioactive components, including alkaloids, flavonoids, tannins, and phenolic compounds[24]. So far, numerous investigations have been conducted on different parts of the *F. communis* plant. According to Rahali et al., the flowers contain ferulic acid and resorcinol, while the stem and fruit consist of ferulic and chlorogenic acids[25]. Generally, polyphenols possess strong antioxidant properties that can protect against neurological diseases, diabetes, cancer, heart disease, and osteoporosis[26]. Furthermore, *F. communis* extracts are rich in ferutinin, which is responsible for many observed effects, including phytoestrogenic, antioxidant, anti-inflammatory, antiproliferative, and cytotoxic properties[27]. Additionally, ferulenol and ferchromone, which were isolated from various parts of *F. communis*, exhibit antibacterial properties[28].

In the current study, a green synthesis method was utilized to produce AgNPs from the aqueous extract of the aerial parts of *F. communis*. During the study, various parameters that influence the size and morphology of the synthesized AgNPs (FC-AgNPs) were optimized. These parameters included the concentration of the plant extract, the reaction time, and the incubation temperature. The as-synthesized FC-AgNPs were characterized using a variety of techniques, including UV-Vis absorption spectroscopy, Fourier-transform infrared spectroscopy (FT-IR), X-ray powder diffraction (XRD), and transmission electron microscopy (TEM). Additionally, the antibacterial and antifungal activities of the nanoparticles were evaluated against several bacterial and fungal pathogens (Fig. 1).

Materials and methods

Plant material

Aerial parts of *F. communis* were collected in March 2024 from Hail located in the northern region of Saudi Arabia, after all required permissions were secured from the relevant authorities. The plant was taxonomically authenticated by Dr. Rajakrishnan Rajagopal at the Herbarium of the Department of Botany, King Saud University, Riyadh. A voucher specimen (KSU-24692) was deposited in the university's herbarium for the record.

Chemicals

All chemicals and solvents used in this study were of analytical-grade. Silver nitrate $AgNO_3$ (99.8%) was obtained from Sigma Aldrich (St. Louis, MO, USA). Other organic solvents such as methanol, continuous series of straight-chain hydrocarbons (C8-C31) used in this work were purchased from Sigma Aldrich and were employed as purchased. Muller Hinton Agar, Nutrient broth, Potato dextrose broth, Amoxicillin and Amphotericin B, all the media and antibiotics were procured from HiMedia Pvt Ltd., Mumbai, India.

Preparation of plant extract

200 g of fresh aerial parts of *F. communis* were chopped into small pieces and soaked in deionized water (2000 mL) and then refluxed for 3 h. The aqueous solution was filtered and further dried in a rotary evaporator at 50 °C under decreased pressure after complete cooling, resulting in 11.6 g of a dark brown powder (FCW)[29]. Initially, 0.1 g/mL of the powdered extract was utilized for the production of FC-AgNPs.

Fig. 1. Schematic representation of synthesis of silver nanoparticles (FC-AgNPs) using an aqueous extract of the *F. communis*.

Synthesis of silver nanoparticles using *F. communis* (FC-AgNPs)

For each experiment, a 1 mM silver nitrate solution was produced by adding a stoichiometric amount of $AgNO_3$ to deionized water. To prepare the reaction mixture, 1 mL of *F. communis* aerial parts extract (FCW) solution was added gradually to 99 mL of 1 mM $AgNO_3$ solution in a 250 mL round-bottom flask, equipped with a cooling condenser and magnetic stir bar. The reaction was sustained for 4 h at 90 °C. The mixture's color changed from pale yellow to reddish brown, confirming the creation of AgNPs. After four hours, no more color change was noticed. Consequently, the mixture was allowed to cool before centrifugation. The centrifugation was subsequently performed at 9000 rpm for 20 min at ambient temperature (25 °C). Subsequently, the reaction product was washed three times with deionized water to yield a black powder, which was then dried in an oven set to 80 °C overnight. The reaction mixture was analyzed by a UV–Vis spectrophotometer during various incubation times, and the absorption peak was detected.

Optimization of different parameters for FC-AgNPs synthesis

Several factors influence the reduction of silver ions to form FC-AgNPs, in addition to the type of plant extract used. The morphology and size of biosynthesized FC-AgNPs primarily depend on reaction parameters including concentration of reactants. It has been observed that smaller spherical AgNPs with minimal aggregation are more effective for most applications[30]. In this study, we investigated the effects of plant extract concentration, incubation temperature, and reaction time on the synthesis of AgNPs.

Temperature effect

The effect of temperature on nanoparticle synthesis was studied by measuring the reaction mixture of plant extract and 1.0 mM $AgNO_3$ at 90 °C and room temperature.

Reaction time effect

The impact of reaction time on the synthesis of silver nanoparticles was examined at various intervals. Therefore, the reaction mixture was examined at different times (0, 5 min, 10 min, 20 min, 40 min, 60 min, 2 h, and 4 h) at 90 °C, while at RT the time intervals were (1 h, 2 h, 3 h, 4 h, 24 h, 48 h, 72 h, and 84 h).

Plant extract concentration

Various experiments were conducted utilizing different concentrations of plant extract (10, 25, 50, 100, 200, 300, and 400 mg) to investigate the effect of plant extract concentration. In each experiment, different concentrations of plant extract were added drop by drop to 1 mM $AgNO_3$ solution. All experiments were conducted at 90 °C.

Characterization of NPs

The prepared AgNPs sample was first examined by a UV-visible spectrophotometer (Shimadzu model UV 1800) in the range of 200–800 nm by using deionized water as a reference solvent in a quartz cuvette. FTIR analyses were carried out by Thermo Scientific NICOLET iS 10 FTIR spectrometer. The transmittance of IR spectra was measured in the region of 4000–500 cm^{-1} at room temperature. Plant extract and AgNPs were combined with KBr separately and formed into a pellet to prepare samples for FTIR analysis. The crystalline nature of AgNPs was determined by using XRD (D2-Phaser, Bruker, Germany) in the 2θ range. The scanning was performed in the range between 20 ºC and 80 ºC of CuKa radiation with λ = 1.54 Å. The shape and size distribution of synthesized silver nanoparticles were characterized by JEM-1011 transmission electron microscopy (JEOL, Tokyo, Japan).

Antimicrobial activity of FC-AgNPs

The antibacterial and antifungal tests of plant extract and synthesized FC-AgNPs were performed against common pathogens, including the gram-positive bacteria *S. aureus* (ATCC12598), and *B. subtilis* (ATCC25922), gram-negative bacteria *E. coli* (ATCC25922), *P. aeruginosa* (ATCC10145), and *K. pneumoniae* (ATCC13883), and fungi *A. niger* (ATCC6275), and *C. albicans* (ATCC2091), using the agar well diffusion method. Both broth culture of bacterial and fungal pathogens was swabbed into Muller Hinton agar (MHA) and made wells were made with sterile cork poorer. The initial well was loaded with 25 µL of FCW (stock concentration of 10 mg/mL), the second well was loaded with 50 µL of FC-AgNPs (stock concentration of 1 mg/mL) and the center well loaded with standard drug for bacteria Amoxicillin (AMX) (10 µL of 1 mg/mL) and for fungi Amphotericin (Amp B) (10 µL of 1 mg/mL) as a positive control with respective pathogens. All the MHA plates were incubated at 24 h and 48 h for bacteria, *C. albicans* and *A. niger* respectively. Later, incubation the mean zone of inhibition (MZI) in millimeters (mm) for each microbial pathogen represents the concentration that exhibits the inhibition zone were calculated[31].

GC-MS analysis of aqueous extract of *F. communis*

To analyze and identify the phytoconstituents of the aqueous extract of *F. communis*. Gas chromatography-mass spectrometry (GC-MS) analysis was performed on an Agilent single quadrupole mass spectrometer with an inert mass selective detector (MSD-5975 C detector, Agilent Technologies, USA). The gas chromatograph was equipped with a split–split less injector, a quick swap assembly, an Agilent model 7693 autosampler, and a HP-5MS fused silica capillary column (5% phenyl 95% dimethylpolysiloxane, 30 m × 0.25 mm i.d., film thickness 0.25 µm, Agilent Technologies, USA). Separation of phytoconstituents were achieved employing previously described methodology with slight modification[32]. In short, injector temperature was maintained at 250 °C with following oven temperature profile: an isothermal hold at 50 °C for 4 min, followed by a ramp of 4 °C/min to 220 °C, an isothermal hold for 2 min, a second ramp to 280 °C at 20 °C/min, and ultimately an isothermal hold for 15 min. For each sample, approximately 0.3 µl diluted in methanol was injected in split mode with a split flow ratio of 10:1. The helium carrier gas used at 1 mL/min. TIC profiles and mass spectra were obtained using the ChemStation data analysis software (version E-02.00.493, Agilent). All mass spectra were acquired in the EI mode (scan range of m/z 45–600 and ionization energy of 70 eV). The ion source and MS quadrupole temperatures were sustained at 230 °C and 150 °C, respectively. The MSD transfer line was sustained at 280 °C for the analyses.

Linear retention indices (LRIs)

The linear retention indices (LRIs) of chemical constituents of *F. communis* extracts were determined using a continuous series of straight-chain hydrocarbons, ranging from C8-C31, was injected using the identical conditions outlined above. LRIs were calculated utilizing the van den Dool and Kratz equation. Calculated LRIs of the phytoconstituents of *F. communis* extract are listed in Table 2.

Identification of phytochemicals of aqueous extract of F. communis

The identification of various phytocomponents in the *F. communis* aqueous extracts was achieved by comparing their mass spectra with entries in mass spectral databases (WILEY 9th edition, NIST-14 MS library, and Adams and Flavor libraries). Additionally, the mass spectra and linear retention indices (LRIs) values of compounds were compared to confirm their identification with published data[33–36].

Statistical analysis

Analysis of variance (ANOVA) and Paired t Test was performed for concentration of inhibition zone to compare the microbial pathogens vs. FCW extract and FC-AgNPs. Means were separated using Duncan's Multiple Range Test (DMRT) (IBM SPSS 20 version).

Results and discussions

UV-Vis analysis

Initially, the formation of NPs from metal ions was visually observed by the change in color of the Ag NP sample's reaction medium. In this study, the addition of the plant solution to the $AgNO_3$ solution caused the color to gradually change from yellow to reddish-brown, indicating the formation of nanoparticles in the colloidal solution (Fig. 2a). The formation of metallic nanoparticles was further confirmed by the UV-Vis absorption peak observed around 400–450 nm (Fig. 2b). According to previous studies, AgNPs that exhibit a spherical shape typically show an absorbance peak at a maximum between 420 nm and 450 nm, displaying only a single peak. In contrast, anisotropic particles display multiple surface plasmon resonance (SPR) bands[37]. In this study, the

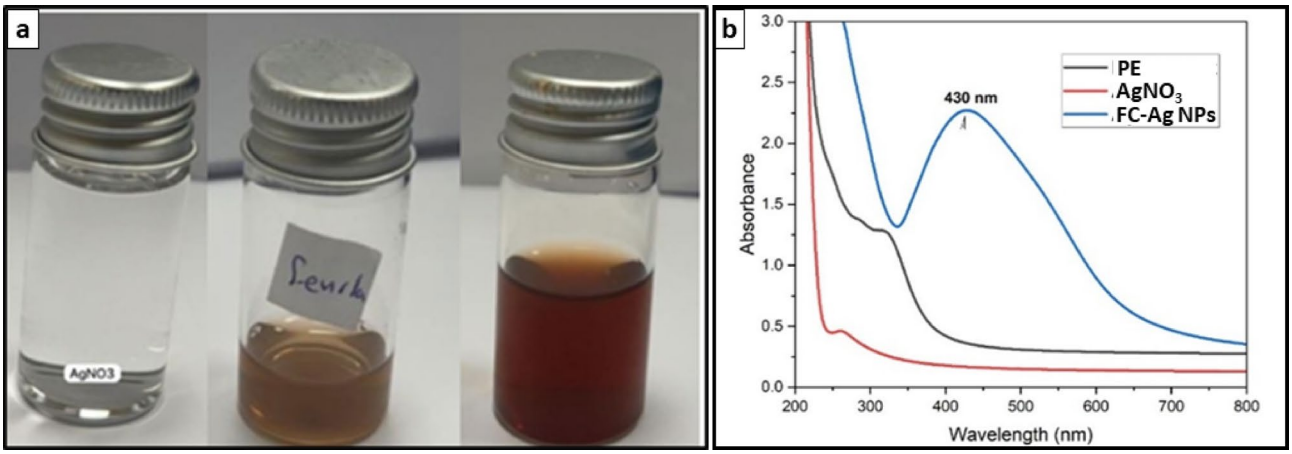

Fig. 2. **(a)** photograph of the aqueous solutions of $AgNO_3$, pure plant extract, and FC-AgNPs colloidal solution; **(b)** UV–Vis spectra of *F. communis* plant extract, $AgNO_3$ and AgNPs.

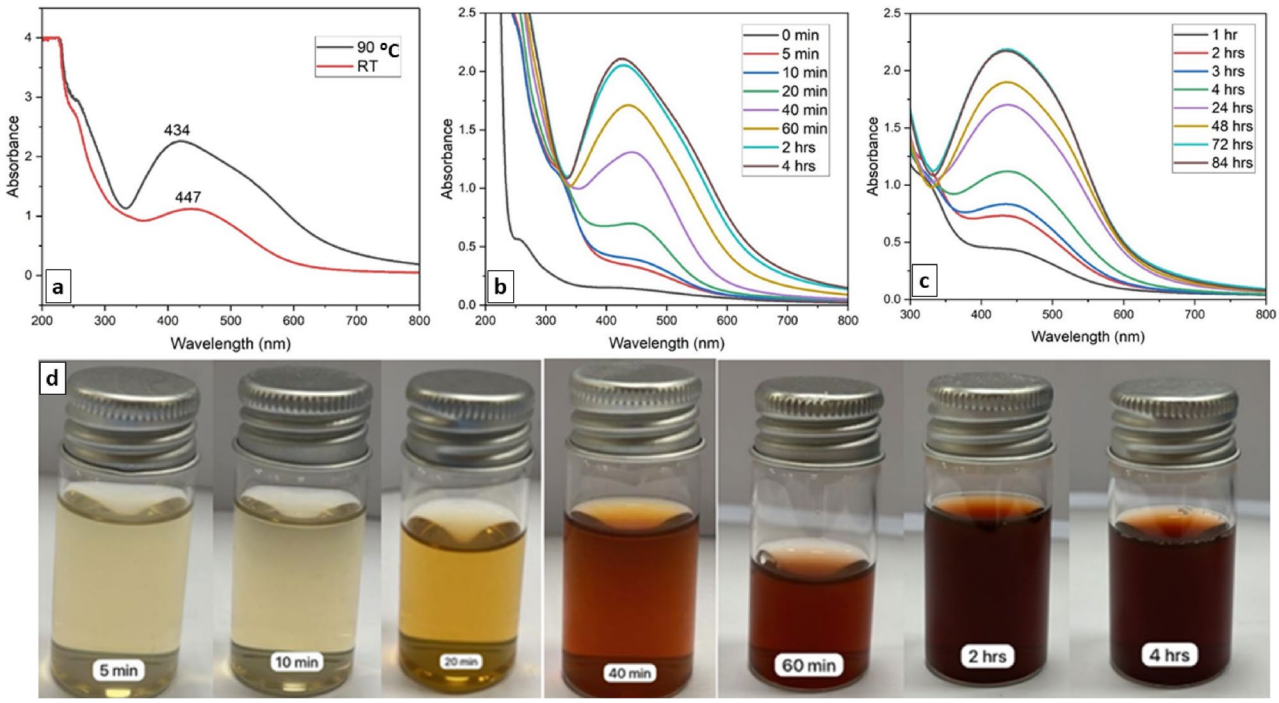

Fig. 3. **(a)** UV-Vis spectra of FC-AgNPs prepared at 90 °C and RT, **(b)** UV-Vis absorption spectra of (FC-AgNPs) prepared at 90° at different interval of time, **(c)** UV-Vis absorption spectra of FC-AgNPs at RT at different interval of time, and **(d)** Images of the colloidal solution of FC-AgNPs demonstrating the change in the color of the solution at 90 °C with increasing time.

FC-AgNPs showed a single peak at the maximum absorbance of 430 nm, confirming the bioreduction of silver ions to AgNPs.

Typically, the synthesized AgNPs are analyzed using UV-Vis spectroscopy to optimize the reaction conditions for improving both the yield and quality of nanoparticles (FC-AgNPs). The effect of temperature was assessed at 90 °C and room temperature (RT), while keeping other variables constant. Figure 3a illustrates that the biosynthesis of FC-AgNPs occurs more rapidly at the higher temperature (90 °C) compared to RT, as increased temperature accelerates the formation of nanoparticles, as indicated by the surface plasmon resonance (SPR) band[38]. The greater intensity of the SPR band for AgNPs produced at 90 °C can be attributed to the higher yield of nanoparticles synthesized at this temperature, as opposed to those produced at room temperature. Additionally, a blue shift in the absorption peak was observed with the increase in temperature, suggesting that smaller particle sizes were produced at 90 °C compared to those at room temperature.

The incubation time of the reaction mixture is a critical variable for enhancing the synthesis of biosynthesized nanoparticles. The UV spectra of freshly prepared FC-AgNPs colloidal solutions were measured at two temperatures: 90 °C and room temperature (RT), over various time intervals. The reaction mixtures were analyzed using UV-Vis spectroscopy at different time points, ranging from 0 min to 4 h at 90 °C and from 0 min to 84 h at RT. At the higher temperature of 90 °C, the intensity of the SPR peak increased with time, indicating the increasing formation of FC-AgNPs (Fig. 3b). As shown in Fig. 3b, a hyperchromic effect was observed at 90 °C, demonstrating a rise in the quantity of silver nanoparticles over time. After 4 h, there was no noticeable change in color, which was reflected in the SPR band. The intensity of the bands gradually increased until around 4 h. The similarity in the bands observed at 2 h and 4 h suggested that the reaction had reached completion. Conversely, the nucleation process at room temperature was significantly slower and required up to 72 h (Fig. 3c). Therefore, the optimal time for the reaction mixture to form silver nanoparticles was determined to be 4 h at 90 °C. Figure 3d demonstrate the visible change in the color of the colloidal solution of AgNPs over time at 90 °C.

The concentration of plant extract is a crucial parameter for optimizing the preparation of AgNPs. To evaluate its effect, various concentrations of plant extract (10 mg, 25 mg, 50 mg, 100 mg, 200 mg, 300 mg, and 400 mg) were tested while keeping all other variables constant (1 mM $AgNO_3$ for 4 h at 90 °C). The results indicated that as the concentration of plant extract increased from 10 mg to 200 mg, the absorbance peak gradually increased, with a blue shift observed from 426 nm to 420 nm. However, when the concentration exceeded 200 mg, a decrease in the absorbance peak was noted, suggesting a reduction in the production of AgNPs. The increase in plant extract concentration significantly affected the formation of NPs, as illustrated in Fig. 4. Higher concentrations (i.e., > 200 mg) of plant extract made the nanoparticles more susceptible to agglomeration and clustering, which in turn decreased the absorption peak due to the formation of larger aggregates[39]. Additionally, the concentration of plant extract plays a pivotal role in determining the size of the nanoparticles. Previous reports have indicated that a broad absorption peak at higher wavelengths typically corresponds to larger particle sizes, while a sharp peak at shorter wavelengths indicates smaller particle sizes. The absorption spectra of FC-AgNPs as shown in Fig. 4 revealed that the maximum absorbance, characterized by a sharp peak at a shorter wavelength (cf. Figure 4, purple line), occurred at a concentration of 200 mg of plant extract, indicating the formation of smaller particles and a higher yield of AgNPs. In contrast, increasing the concentration of plant extract to 300 mg and 400 mg resulted in a decrease in the absorption peak.

XRD analysis

The XRD pattern presented in the Fig. 5 provides valuable crystallographic information about the composition and structure of the FC-AgNPs. The XRD pattern reveals a mixed-phase material containing metallic AgNPs and other additional phase, with distinctive diffraction peaks of Ag corresponding to its respective crystallographic planes. The diffractogram displays several well-defined diffraction peaks with varying intensities, the most prominent peak appears at approximately 38° which can be indexed to silver (111), exhibiting the highest

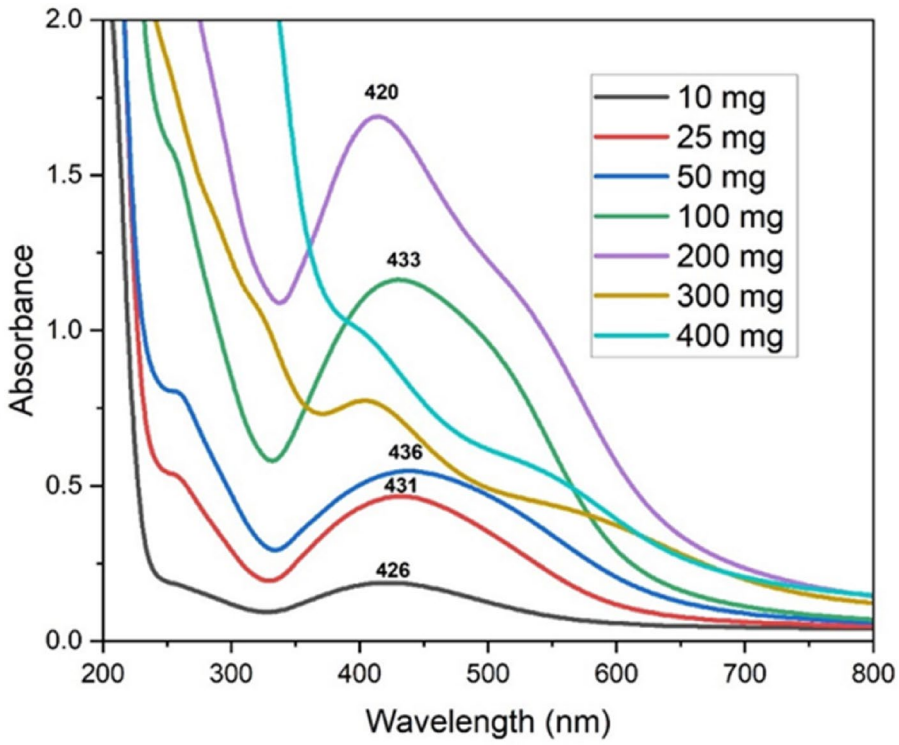

Fig. 4. UV-Vis absorption spectra of FC-AgNPs prepared at various concentrations of plant extract at 90 °C.

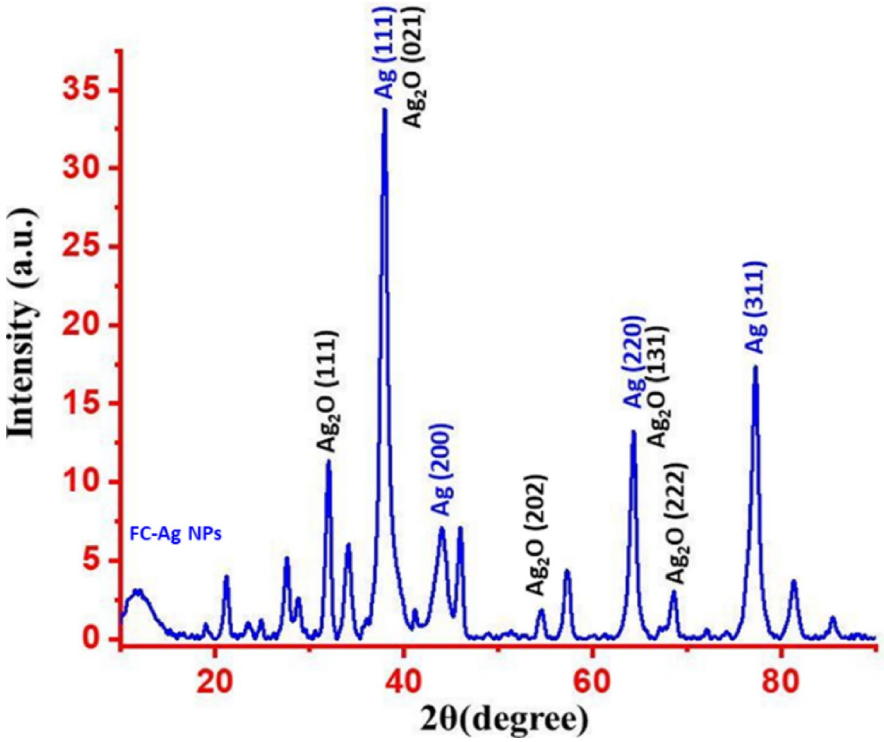

Fig. 5. XRD pattern of the silver nanoparticles (FC-AgNPs).

intensity. The diffraction pattern reveals a face-centered cubic (*fcc*) crystal structure typical of AgNPs, with characteristic peaks corresponding to the ~ 37.6 (111), ~ 44.2° (200), ~ 63.9° (220), and ~ 76.8° (311) planes of metallic silver. This crystal phase matches well with the standard JCPDS card (04–0783) for metallic silver[40]. Concurrently, in addition to the prominent peaks of Ag, several other peaks also appear in the diffractogram, which closely resembles to the characteristic peaks of silver oxide phase (Ag_2O)[41]. The peaks at 2θ values of approximately 32.9° (111), 38.2° (200), 55.1° (220), 66.0° (311), and 69.2° (222), which align well with the standard JCPDS file No. 41–1104 for cubic Ag_2O[42]. The presence of multiple Ag_2O peaks indicates partial oxidation of the AgNPs, which is a common phenomenon when AgNPs are exposed to air or during certain synthesis processes. The relative intensities of the peaks suggest that both phases are present in significant amounts, with the metallic silver potentially being the dominant phase based on the high intensity of the Ag (111) peak. The distinct diffraction peaks indicate high crystallinity, suggesting well-formed crystalline nanoparticles instead of amorphous structures.

TEM analysis

The image displayed in Fig. 6 presents a detailed transmission electron microscopy (TEM) characterization of FC-AgNPs alongside their size distribution analysis. The NPs exhibit a mean diameter of 26.64 ± 1.02 nm with a relatively narrow size distribution, indicating a well-controlled synthesis process. The TEM image reveals predominantly spherical particles with some degree of aggregation, which is characteristic of AgNPs due to their surface properties and high surface energy. The nanoparticles demonstrate varying degrees of aggregation throughout the sample. Some regions show densely packed clusters while others display more dispersed individual particles. This heterogeneous distribution suggests potential challenges in achieving complete colloidal stability, which is a common issue with AgNPs suspensions[43]. The contrast differences between particles may indicate variations in thickness, crystallinity, or orientation relative to the electron beam. The boundaries between individual particles within aggregates remain distinguishable, suggesting limited fusion or sintering between particles. The histogram on the right-hand side of TEM image in Fig. 6 provides quantitative size analysis of the AgNPs. The distribution data reveals that the NPs have a mean length (diameter) of 26.64 ± 1.02 nm, where 1.02 nm represents the standard deviation. This relatively small standard deviation (approximately 3.8% of the mean) indicates a narrow size distribution and suggests good control over the particle synthesis process. The observed size distribution of AgNPs has important implications for their potential applications. With a mean diameter of 26.64 nm, these particles fall within the optimal size range for several biomedical and catalytic applications. At this size range, AgNPs typically exhibit strong surface plasmon resonance effects, which enhance their antimicrobial properties and optical sensing capabilities.

FTIR analysis

The dual role of the *F. communis* extract as a reducing and stabilizing agent was confirmed through FT-IR analysis of the prepared FC-AgNPs. Figure 7 displays FT-IR spectra comparing a *F. communis* plant extract

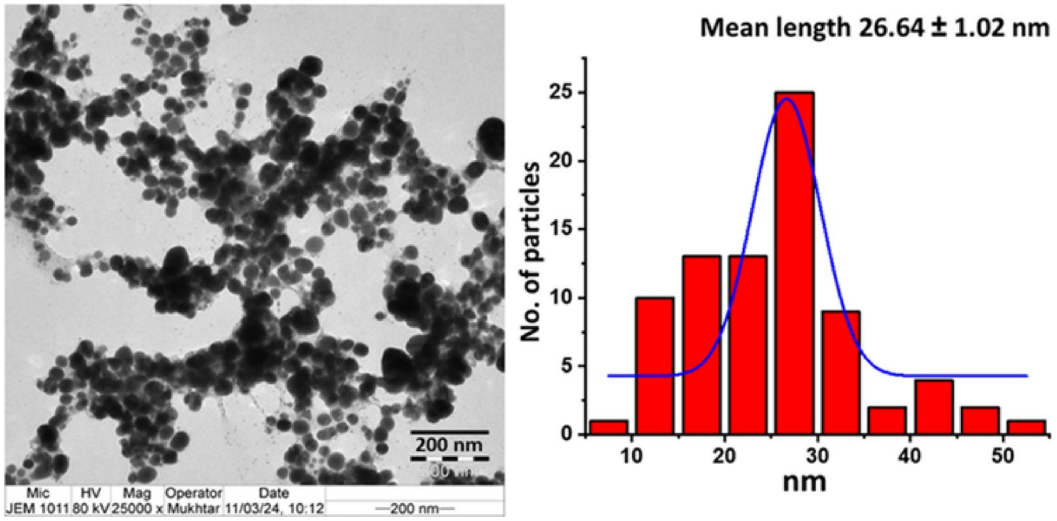

Fig. 6. TEM images at different scales and particle size distribution of (FC-AgNPs).

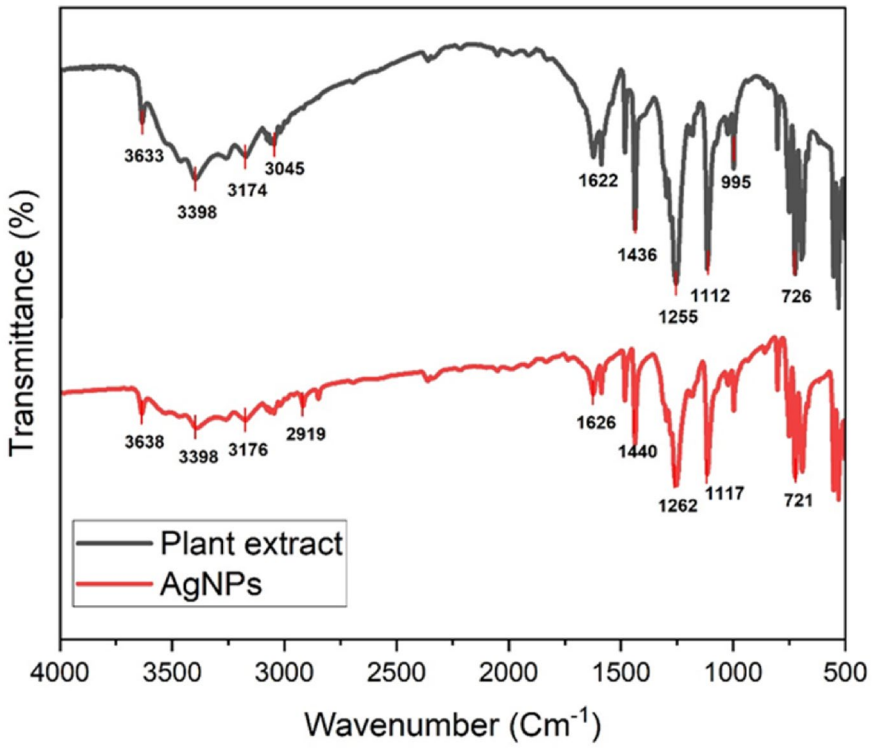

Fig. 7. FTIR spectra of synthesized (FC-AgNPs), and *F. communis* plant extract.

(black line) with FC-AgNPs (red line). This spectroscopic comparison reveals important information about the functional groups present in the plant extract and how they interact with Ag during NPs formation. *F. communis*, commonly known as giant fennel, contains various bioactive compounds including phenolic acids and flavonoids that likely contribute to its medicinal properties. The high wavenumber region reveals several significant peaks related to hydroxyl and hydrocarbon functional groups in the plant extract. The peak at 3633 cm^{-1} in the plant extract (3638 cm^{-1} in AgNPs) corresponds to the stretching vibrations of free hydroxyl groups (-OH) from alcohols and phenols, indicating the presence of polyphenolic compounds[44]. The strong absorption at 3398 cm^{-1}, which is identical in both spectra, can be attributed to the hydrogen-bonded OH stretching vibrations that are characteristic of polyphenolic compounds and other molecules containing hydroxyl groups. The peaks at 3174 cm^{-1} (from plant extract) and 3176 cm^{-1} (from AgNPs) likely correspond to N-H stretching vibrations

of primary or secondary amines and amides, suggesting the presence of nitrogen-containing compounds in *F. communis*.

The peak at 3045 cm^{-1} in the plant extract spectrum indicates aromatic C-H stretching, suggesting the presence of aromatic compounds such as phenolics. This is consistent with the expected phytochemical profile of *F. communis* plants, which are known to contain various aromatic compounds[45]. The peak observed at 1622 cm^{-1} in the plant extract (and at 1626 cm^{-1} in the AgNPs) indicates the presence of C = C double bonds from aromatic rings or possibly C = O stretching vibrations. This further suggests the existence of aromatic compounds and potentially carbonyl-containing structures, such as flavonoids or phenolic acids. Additionally, the absorption detected at 1436 cm^{-1} in the plant extract and at 1440 cm^{-1} in the AgNPs can be attributed to C-H bending vibrations in methyl or methylene groups that are attached to aromatic rings. This implies the presence of methylated aromatic compounds in the *F. communis* extract. The peak at 1255 cm^{-1} (1262 cm^{-1} in AgNPs) likely corresponds to C-O stretching vibrations in phenols, ethers, or esters. This aligns with the presence of phenolic compounds that contain C-O bonds. The absorption at 1112 cm^{-1} (1117 cm^{-1} in AgNPs) can be assigned to C-O-C stretching vibrations in ethers or C-OH stretching in alcoholic groups.

The peak at 995 cm^{-1} in the plant extract may represent = C-H out-of-plane bending vibrations in alkenes or C-O stretching in polysaccharides. This suggests the presence of unsaturated compounds or carbohydrate structures in the extract. The absorption at 726 cm^{-1} (721 cm^{-1} in AgNPs) falls within the range for C-H out-of-plane bending vibrations in aromatic compounds (850–670 cm^{-1}), further confirming the presence of aromatic structures in the *F. communis* extract. The FT-IR spectra of the plant extract and the FC-AgNPs show notable similarities in peak positions, albeit with some subtle shifts and variations in intensity. These similarities suggest that the biomolecules from the *F. communis* extract play a role in the reduction and stabilization of AgNPs. The minor shifts in peak positions between the plant extract and the AgNPs (for example, from 1622 to 1626 cm^{-1} and from 1255 to 1262 cm^{-1}) likely indicate interactions between the functional groups in the plant extract and silver ions during the formation of the NPs. These interactions typically involve oxygen-containing functional groups, such as hydroxyl and carboxyl groups, which can reduce silver ions and subsequently stabilize the generated NPs.

Notably, the subtle peak shifts observed between plant extract and nanoparticle spectra (e.g., 1622→1626 cm^{-1} and 726→721 cm^{-1}) demonstrate clear evidence of molecular interactions between functional groups and silver ions during reduction and stabilization (Table 1). This phenomenon is consistent with findings from other plant-mediated silver nanoparticle studies, where FTIR analysis confirms that polyphenolic compounds, flavonoids, and terpenoids serve dual roles as both reducing and capping agents[46]. For instance, the hydroxyl group stretching vibrations appear in comparable regions in both studies which reports peaks at 3633 cm^{-1} and 3398 cm^{-1}, while *P. dulce* extracts show O-H stretching around 3770 cm^{-1}. The presence of aromatic C-H stretching (3045 cm^{-1} in FC-AgNPs vs. 2920 cm^{-1} in *P. dulce*) and carbonyl groups (1622–1626 cm^{-1} for FC-AgNPs vs. 1736 cm^{-1} for *P. dulce*) confirm the involvement of phenolic compounds and organic acids in both biosynthesis processes. The comparative analysis underscores how different plant extracts contribute unique phytochemical signatures that influence nanoparticle characteristics, stability, and ultimately their biological activities.

Chemical constituents identification from the aqueous extract of *F. communis*

To identify the chemical constituents of the water extract from *F. communis*, a GC-MS analysis was conducted. This analysis revealed a total of 67 compounds, which accounted for 88.4% of the overall composition (see Table 2).

The extract was primarily composed of oxygenated aliphatic hydrocarbons (30.9%), sterols (18.2%), oxygenated sesquiterpenes (9.7%), and diterpenoids (7.7%). Notably, the most dominant compounds identified were stigmasterol, pentadecanoic acid, (5*E*, 9*Z*)-farnesyl acetone, and pentyl docosanoate (Fig. 8),

S. No.	Peak value wavenumber (cm^{-1})	Functional group assignment	Attribution	Role in the synthesis
1	3633 (PE)/3638 (AgNPs)	O-H stretching	Free hydroxyl groups from alcohols and phenols	Reducing and stabilizing agent
2	3398	O-H stretching (hydrogen-bonded)	Polyphenolic compounds with hydroxyl groups	Reduction of Ag^+ ions
3	3174 (PE)/3176 (AgNPs)	N-H stretching	Primary or secondary amines and amides	Stabilization of nanoparticles
4	3045	Aromatic C-H stretching	Aromatic compounds (phenolics)	Phytochemical marker
5	1622 (PE)/1626 (AgNPs)	C = C stretching/C = O stretching	Aromatic rings/carbonyl groups (flavonoids, phenolic acids)	Electron donation for silver reduction
6	1436 (PE)/1440 (AgNPs)	C-H bending	Methyl/methylene groups attached to aromatic rings	Structural component of phytochemicals
7	1255 (PE)/1262 (AgNPs)	C-O stretching	Phenols, ethers, or esters	Capping and stabilizing agent
8	1112 (PE)/1117 (AgNPs)	C-O-C stretching/C-OH stretching	Ether linkages or alcoholic groups	Nanoparticle stabilization
9	995	C-H out-of-plane bending/C-O stretching	Unsaturated compounds or polysaccharides	Supporting reducing activity
10	726 (PE)/721 (AgNPs)	C-H out-of-plane bending (aromatic)	Aromatic structures	Structural marker of plant extract

Table 1. FT-IR peak values, their corresponding functional groups and attributions. PE = Plant extract; AgNPs = Silver nanoparticles.

S. No.	Compounds*	M.F.	M.W.	CAS No.	*R*.T. (min)	LRI_{Lit}	LRI_{Exp}	%[b]
1	2-Hydroxy-2-cyclopenten-1-one	$C_5H_6O_2$	98	10493-98-8	7.112	927	924	0.4
2	3-Methylbutyl butanoate	$C_9H_{18}O_2$	158	106-27-4	12.17	1052	1059	0.1
3	Ethylbenzoate	$C_9H_{10}O_2$	150	93-89-0	16.376	1169	1171	0.2
4	Terpinen-4-ol	$C_{10}H_{18}O$	154	562-74-3	16.581	1174	1176	0.1
5	Methyl salicylate	$C_8H_8O_3$	152	119-36-8	17.111	1190	1190	0.2
6	*n*-Decanol	$C_{10}H_{22}O$	158	112-30-1	20.122	1266	1275	0.5
7	Hexyl pentanoate	$C_{11}H_{22}O_2$	186	1117-59-5	20.873	-	1297	t
8	4-Methylhexyl-3-methylbutanoate	$C_{12}H_{24}O_2$	200	1215127-80-2	21.138	-	1304	t
9	2-Methoxy-4-vinylphenol	$C_9H_{10}O_2$	150	7786-61-0	21.362	1309	1311	1.2
10	*δ*-Terpinyl acetate	$C_{12}H_{20}O_2$	196	93836-50-1	21.58	1316	1318	0.1
11	Heptyl 2-methylbutanoate	$C_{12}H_{24}O_2$	200	50862-12-9	22.034	-	1331	0.4
12	Ethyldihydrocinnamate	$C_{11}H_{14}O_2$	178	2021-28-5	22.396	-	1342	0.5
13	*iso*-Butyl octanoate	$C_{12}H_{24}O_2$	200	5461-06-3	22.611	-	1349	0.9
14	*cis*-Geranyl acetate	$C_{12}H_{20}O_2$	196	141-12-8	23.035	1359	1361	0.9
15	*(Z)*-Ethylcinnamate	$C_{11}H_{18}O_2$	176	4610-69-9	23.428	1376	1373	2.0
16	Daucene	$C_{15}H_{24}$	204	16661-00-0	23.617	1380	1379	1.5
17	*β*-Maaliene	$C_{15}H_{24}$	204	489-29-2	23.752	-	1383	1.6
18	*β*-Bourbonene	$C_{15}H_{24}$	204	5208-59-3	23.877	1387	1387	0.7
19	*β*-Elemene	$C_{15}H_{24}$	204	515-13-9	23.962	1389	1389	0.9
20	3-Dodecanone	$C_{12}H_{24}O$	184	1534-27-6	24.066	1389	1393	1.2
21	*n*-Tetradecane	$C_{14}H_{30}$	198	629-59-4	24.215	1400	1397	1.9
22	Dodecanal	$C_{12}H_{24}O$	184	112-54-9	24.404	1408	1403	2.3
23	*β*-Funebrene	$C_{15}H_{24}$	204	79120-98-2	24.549	1413	1408	1.7
24	***cis-threo*-Davanafuran**	**$C_{14}H_{20}O$**	**220**	**54750-65-1**	**24.68**	**1414**	**1412**	**3.1**
25	4-Methoxybenzoic acid	$C_8H_8O_3$	152	100-09-4	25.307	-	1432	0.3
26	3,4-Dehydro-β-ionone	$C_{13}H_{18}O$	190	1203-08-3	26.842	-	1481	0.2
27	Nerolidol	$C_{15}H_{26}O$	222	142-50-7	29.332	1561	1564	0.2
28	*β*-Eudesmol	$C_{15}H_{26}O$	222	473-15-4	31.834	1649	1651	0.1
29	*7-epi-α*-eudesmol	$C_{15}H_{26}O$	222	123123-38-6	32.111	1662	1661	0.8
30	Tridecanoic acid	$C_{13}H_{26}O_2$	214	638-53-9	32.27	-	1666	0.4
31	*trans*-Calamenene-10-ol	$C_{15}H_{22}O$	218	123931-36-2	32.412	1668	1671	0.2
32	Shyobunol	$C_{15}H_{26}O$	222	35727-45-8	32.959	1688	1691	0.1
33	*trans*-Farnesol	$C_{15}H_{26}O$	222	106-28-5	33.715	1742	1719	0.2
34	*trans*-Coniferyl alcohol	$C_{10}H_{12}O_3$	180	32811-40-8	34.234	1733	1738	0.3
35	*(Z)-β*-Curcumen-12-ol	$C_{15}H_{24}O$	220	698365-10-5	34.418	1754	1745	0.6
36	*α*-Costol	$C_{15}H_{24}O$	220	65018-15-7	35.139	1773	1772	2.0
37	Aristolone	$C_{15}H_{22}O$	218	6831-17-0	35.323	1762	1779	1.9
38	Ethyl tetradecanoate	$C_{16}H_{32}O_2$	256	124-06-1	35.616	1795	1790	1.7
39	6,10,14-Trimethyl-2-pentadecanone	$C_{18}H_{36}O$	268	502-69-2	36.889	-	1839	0.5
40	Lauric acid, 2-methylbutyl ester	$C_{17}H_{34}O_2$	270	93815-53-3	37.217	-	1852	0.2
41	**Pentadecanoic acid**	**$C_{15}H_{30}O_2$**	**242**	**1002-84-2**	**38.049**	**-**	**1885**	**7.6**
42	**(5*E*, 9*Z*)-Farnesyl acetone**	**$C_{18}H_{30}O$**	**262**	**3953-35-3**	**38.135**	**1886**	**1888**	**4.5**
43	2-Heptadecanone	$C_{17}H_{34}O$	254	2922-51-2	38.568	-	1905	2.1
44	*(E, E)*-Farnesyl acetone	$C_{18}H_{30}O$	260	1117-52-8	38.857	1913	1917	1.2
45	Methyl hexadecanoate	$C_{17}H_{34}O_2$	270	112-39-0	39.003	1921	1923	1.3
46	*cis*-Hexadec-9-enoic acid	$C_{16}H_{30}O_2$	254	373-49-9	39.665	-	1950	2.1
47	Hexadecanoic acid	$C_{16}H_{32}O_2$	256	57-10-3	39.81	1959	1956	1.1
48	*n*-Heptadecanol	$C_{17}H_{36}O$	257	1454-85-9	40.391	-	1980	0.6
49	*n*-Eicosane	$C_{20}H_{42}$	283	112-95-8	40.873	2000	2000	0.8
50	Abietatriene	$C_{20}H_{30}$	270	19407-28-4	42.03	2055	2050	1.3
51	Phytol	$C_{20}H_{40}O$	297	150-86-7	43.382	1942	2108	0.7
52	3,3'-Di-tert-butyl-5,5'-dimethyl-2,2-dihydroxydiphenylmethane	$C_{23}H_{32}O_2$	340	119-47-1	50.257	-	2414	0.2
53	*n*-Pentacosane	$C_{25}H_{52}$	353	629-99-2	51.845	2500	2501	0.7
54	Bis(2-ethylhexyl) phthalate	$C_{24}H_{38}O_4$	391	117-81-7	52.485	-	2544	1.2
55	Bis(2-ethylhexyl) phthalate	$C_{24}H_{38}O_4$	391	117-81-7	52.581	-	2551	0.7
56	Hexacosane	$C_{26}H_{54}$	367	630-01-3	53.336	2600	2602	0.8

Continued

S. No.	Compounds*	M.F.	M.W.	CAS No.	*R*.T. (min)	LRI_{Lit}	LRI_{Exp}	%[b]
57	Heptacosane	$C_{27}H_{56}$	381	593-49-7	54.559	2700	2697	0.9
58	(*Z*)-9-Octadecenal	$C_{18}H_{34}O$	266	2423-10-1	54.708	-	2709	0.3
59	*iso*-Butyl docosanoate	$C_{26}H_{52}O_2$	397	1000405-17-1	55.084	-	2739	0.2
60	Octacosane	$C_{28}H_{58}$	395	630-02-4	55.839	2800	2798	0.1
61	**Pentyl docosanoate**	**$C_{27}H_{54}O_2$**	**411**	**111-02-4**	**56.245**	**-**	**2830**	**3.5**
62	*n*-Hexacosanol	$C_{26}H_{54}O$	383	506-52-5	56.726	-	2867	1.5
63	Nonacosane	$C_{29}H_{60}$	409	630-03-5	57.138	2900	2899	0.2
64	Pentyl tetracosanoate	$C_{29}H_{58}O_2$	438	28891-27-2	58.266	-	2988	1.4
65	Triacontane	$C_{30}H_{62}$	423	638-68-6	58.447	3000	3002	2.0
66	Fumaric acid, 3-methylbut-2-yl nonadecyl ester	$C_{28}H_{52}O_4$	452	-	58.718	-	3023	1.1
67	**Stigmasterol**	**$C_{29}H_{48}O$**	**412**	**83-48-7**	**60.72**	**-**	**3179**	**18.2**
Oxygenated monoterpenes								1.1
Sesquiterpene hydrocarbons								6.4
Oxygenated sesquiterpenes								9.7
Diterpenoids								7.7
Aliphatic hydrocarbons								7.4
Oxygenated aliphatic hydrocarbons								30.9
Aromatics								4.4
Sterols								18.2
Others								2.6
Total identified								88.4

Table 2. Chemical constituents and their contents detected in the aqueous extract of *F. communis* aerial parts. *Compounds are recorded as per their order of elution from HP-5MS column; b=percentages calculated from MS data and compounds higher than 3.0% are highlighted in boldface; LRI_{Lit} = Linear retention index from the literature[36]; LRI_{Exp}=Computed LRI with reference to *n*-alkanes mixture (C8-C31) on HP-5MS column; t = trace (< 0.05%).

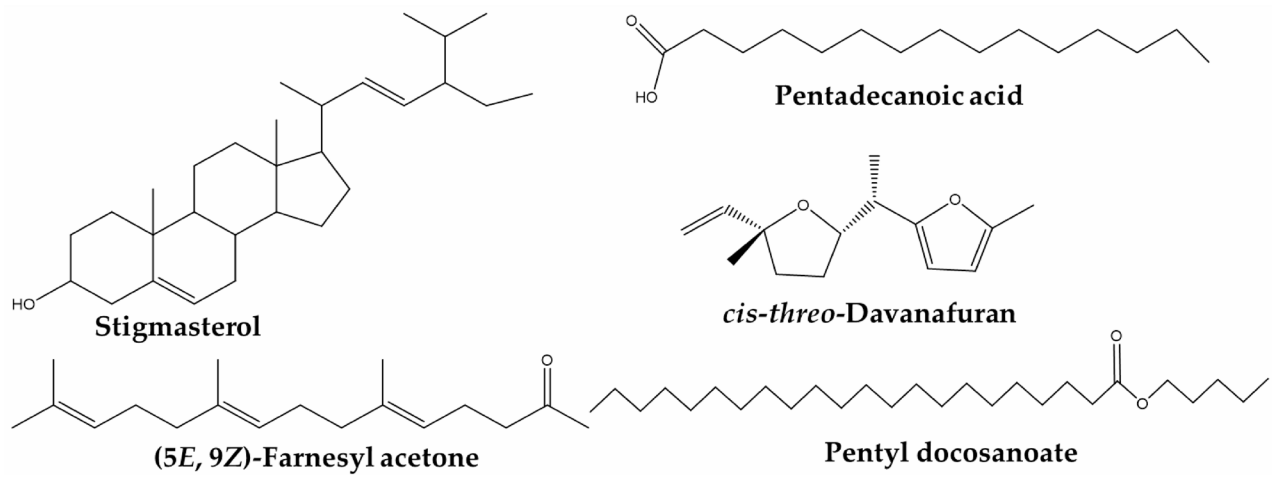

Fig. 8. Chemical structures of the dominating compounds from the aqueous extracts of *F. communis* aerial parts.

which highlight the extract's potential as a reducing and stabilizing agent for nanoparticle synthesis, due to their functional groups and redox properties. Chemical structural representations of the dominating identified compounds appear in Fig. 8, with their chromatographic elution pattern demonstrated in Fig. 9.

Some of the major compound classes identified in aqueous extract of *F. communis* and their possible roles are as follows: phenolic derivatives like 2-Methoxy-4-vinylphenol (1.2%), methyl salicylate (0.2%) and 4-methoxybenzoic acid (0.3%) are phenolic esters/acids with hydroxyl and carbonyl groups. These act as reducing agents for metal ions (e.g., Ag^{+}, Au^{3+}) by donating electrons, facilitating nucleation of nanoparticles[47]. While, 2-methoxy-4-vinylphenol and vanillic acid derivatives provide stabilization via aromatic rings and hydroxyl groups, preventing nanoparticle aggregation[48]. Terpenoids, such as β-Eudesmol (0.1%), nerolidol (0.2%), and *trans*-farnesol (0.2%) are sesquiterpenes with hydroxyl groups that stabilize nanoparticles through

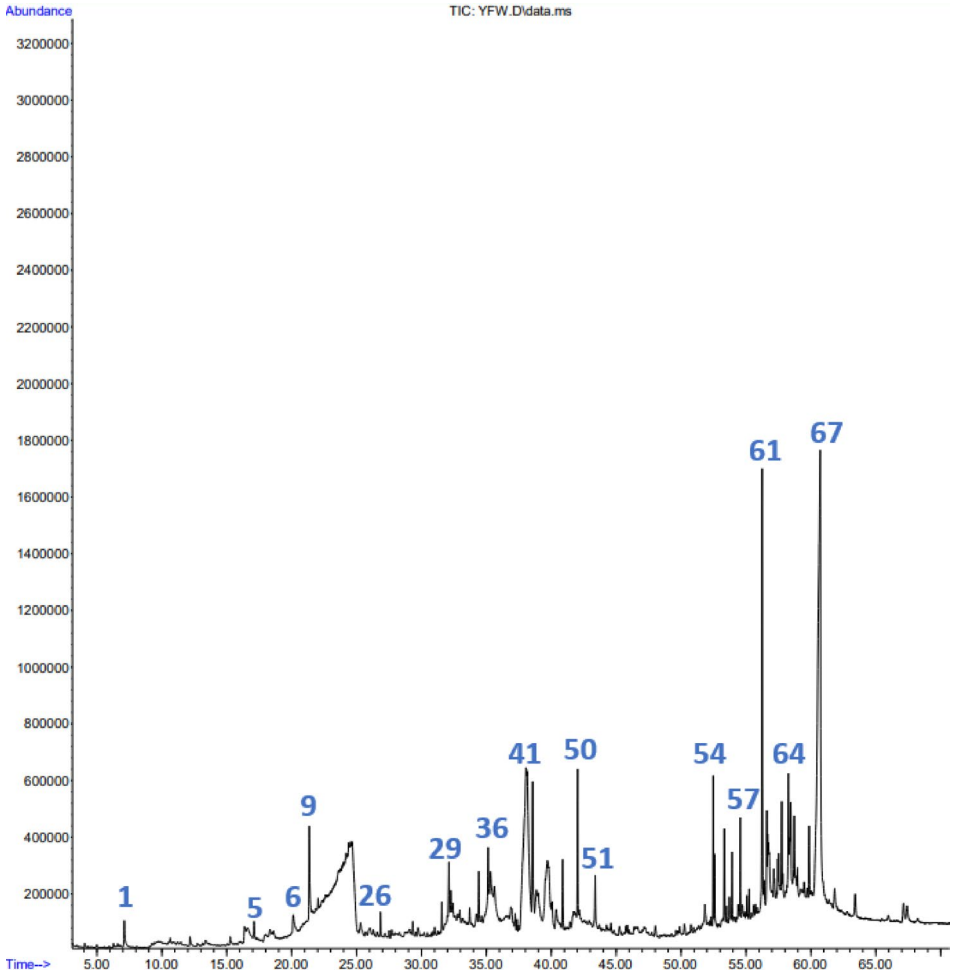

Fig. 9. Total ion chromatogram of water extract of *F. communis* aerial parts.

Compound Class	Role in Synthesis	*F. communis compounds*
Phenolics	Reducing and stabilizing agents	2-Methoxy-4-vinylphenol
Terpenoids	Stabilizing agents	*β*-Eudesmol, *trans*-farnesol
Aliphatic alcohols	Size control	Phytol, *n*-Decanol, *n*-heptadecanol
Sterols	Reducing agent, morphology control	Stigmasterol

Table 3. Possible comparative relevance of the identified components in the aqueous extract of *F. communis* to green synthesis of FC-AgNPs.

steric hindrance and hydrogen bonding. Hydrocarbon sesquiterpenes, including daucene (1.5%) and *β*-elemene (0.9%), may play a crucial role in controlling nanoparticle morphology[49]. Meanwhile, the aliphatic compounds including *n*-decanol (0.5%), *n*-tetradecane (1.9%), hexadecanoic acid (1.1%) and ethyl tetradecanoate (1.7%) due to their long alkyl chains provide hydrophobic environments for controlling nanoparticle size during synthesis and may act as capping agents. The most abundant component in the extract belongs to the class of sterols, such as stigmasterol (18.2%), which is a phytosterol that offers a rigid tetracyclic structure, stabilizing nanoparticles through hydrophobic interactions. The phytosterol is also recognized for its role in the green synthesis of metallic nanoparticles, due to its hydroxyl groups that help in the reduction of Ag^{+} ions to Ag^{0}[50]. Phenolics, such as 2-Methoxy-4-vinylphenol, and alcohols like *n*-decanol (0.5%), may facilitate the reduction of metal ions by donating electrons, which initiates the process of nucleation. In terms of stabilization, terpenoids and sterols possibly adhere to the surfaces of nanoparticles, preventing their aggregation through both steric and electrostatic effects. Moreover, the combination of oxygenated aliphatics (30.9%) and aromatics (4.4%) may improves the solubility and dispersion of nanoparticles in aqueous media (cf. Table 3).

Possible Bio-Reduction of Ag ions

The water extract from *F. communis* contains various phytochemicals, including polyphenols, flavonoids, sterols, alkaloids, and terpenoids. Gas chromatography-mass spectrometry (GC-MS) analysis has confirmed the presence of phenolic acids, terpenoids, sterols, and aliphatic alcohols. However, some other phytoconstituents, such as flavonoids and additional polyphenols, could not be identified due to the technical limitations of GC-MS analysis. These phytochemicals play a crucial role in reducing and stabilizing silver ions into AgNPs. Several studies have shown that different types of polyphenolic compounds and other hydroxyl (OH)-bearing constituents are primarily responsible for the reduction and stabilization of AgNPs[51,52]. The reaction scheme illustrated in Fig. 10 depicts a multi-step process that begins with silver nitrate ($AgNO_3$) interacting with hydroxyl-bearing compounds in their enol form. These reducing constituents possess multiple hydroxyl groups that act as electron donors during the reduction process. In the initial reduction step, hydroxyl-bearing compounds, including polyphenols, transfer electrons to silver ions (Ag^+). This transfer results in the reduction of the silver ions while the phenolic compounds are oxidized, leading to the formation of an unstable intermediate state. The unstable intermediate quickly transforms into a quinone form (keto), which represents the oxidized state of the reducing agent. At the same time, the reduced silver atoms start to aggregate, forming AgNPs nuclei. This process continues as these nuclei grow through cluster formation, eventually developing into larger nanoparticle structures. In the final stage, an organic layer of residual phytoconstituents forms around the AgNPs, providing stabilization and preventing unwanted aggregation.

Biological activity

Antimicrobial resistance has been a major issue globally in recent years, with microorganisms increasingly demonstrating resistance to basic medications used to treat severe illnesses. Nonetheless, a wide range of chemical and green-produced nanoparticles are investigated worldwide. Currently, scientists are interested in using nanoparticles for biological activity. Previous studies have shown nanoparticle formation, either chemically or eco-friendly, prevents the growth of microorganisms like bacteria by influencing bacterial membranes[53,54]. In the current study, the antimicrobial activity of FC-AgNPs and the plant extract was examined against gram-positive *(S. aureus*, and *B. subtilis*), gram-negative bacteria (*E. coli*, *P. aeruginosa*, and *K. pneumoniae*), and fungi (*C. albicans*, and *A. niger*). The results showed the antimicrobial activity of FC-AgNPs against microbial pathogens as shown in Table 4; Fig. 11. FC-AgNPs revealed moderate inhibitory activity compared to standard drugs against bacterial and fungal pathogens (Fig. 12). The maximum inhibition zone was observed against *S. aureus* (10.05 ± 0.05 mm) followed by *E. coli* (9.25 ± 0.05), *C. albicans* (8.70 ± 0.05*)*, *P. aeruginosa (*8.50 ± 0.20*)*,

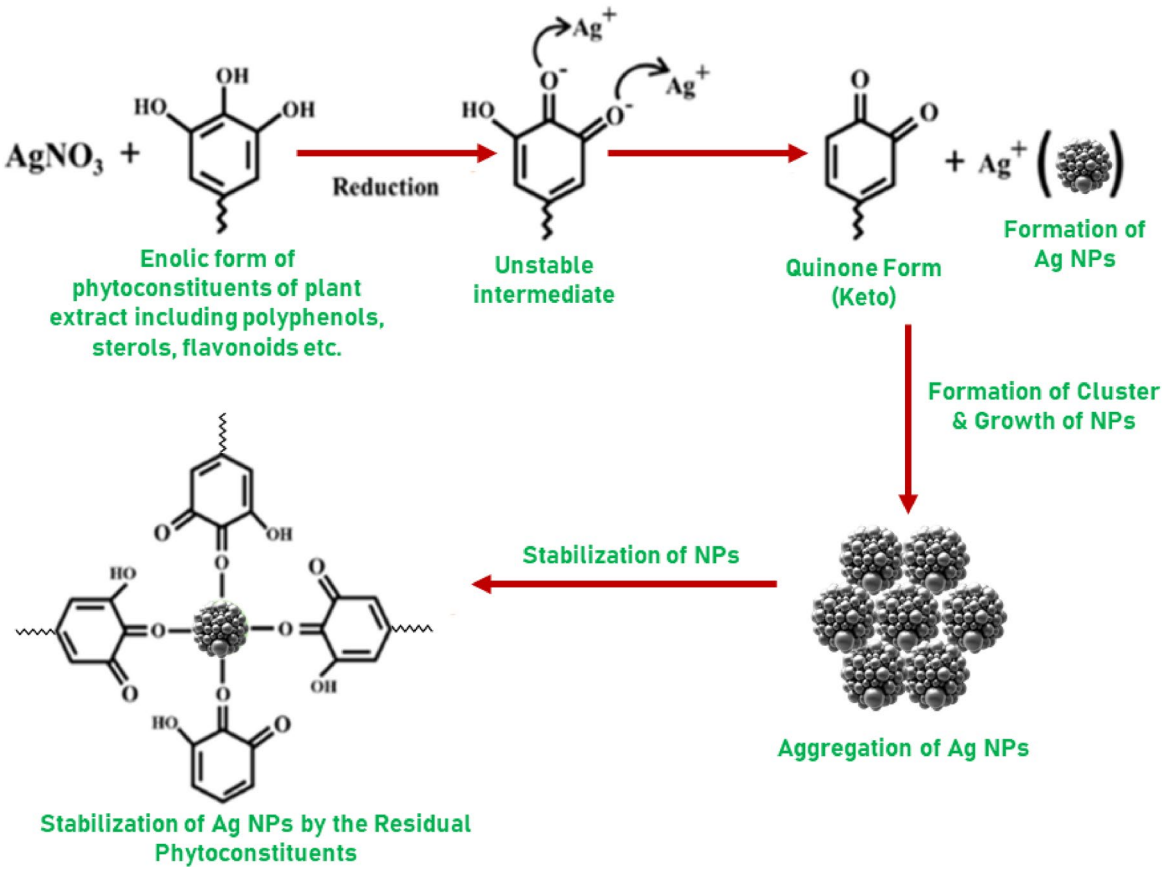

Fig. 10. Schematic representation of the possible reaction pathway for the formation of FC-AgNPs by the contribution of phytoconstituents of *F. communis* extract[51].

Microbial pathogens	Concentration/Inhibition zone (mm)		Standard Drug
	FCW (25 µL) (10 mg/mL)	FC-AgNPs (50 µL) (1.0 mg/mL)	AMX (10 µL) (1.0 mg/mL)
Gram positive bacteria			
S. aureus ATCC12598	#2.33 ± 2.33	9.93 ± 0.22[a]	20.00
B. subtilis ATCC6051	2.17 ± 2.17	7.75 ± 0.42[d]	18.00
Gram negative bacteria			
E. coli ATCC25922	7.23 ± 0.43	9.33 ± 0.22[ab]	21.00
aeruginosa ATCC10145	2.72 ± 2.72	8.37 ± 0.09[cd]	19.50
K. pneumoniae ATCC13883	2.25 ± 2.25	8.10 ± 0.13[cd]	17.00
Fungi			**Amp B (10 µL) (1.0 mg/mL)**
C. albicans ATCC2091	2.23 ± 2.23	8.47 ± 0.15[cd]	17.50
A. niger ATCC6275	4.60 ± 2.31	8.73 ± 0.16[bc]	16.00
$F_{6,14}$	0.773ns	11.347***	
Concentration $_{(1'28)}$ Microbes $_{(6,28)}$ Concentration ×Microbes$_{(6,28)}$		41.282*** 1.127ns 0.637ns	

Paired Samples Test

		Paired Differences					t	df	Sig. (2-tailed)
		Mean	Std. Deviation	Std. Error Mean	95% Confidence Interval of the Difference Lower	Upper			
Pair 1	**VAR00007 - VAR00008**	**−5.30714**	**1.74573**	**0.65983**	**−6.92168**	**−3.69261**	**−8.043**	**6**	**0.000**

Table 4. Antimicrobial activity of FCW extract and FC-AgNPs against microbial pathogens. #Each value is a mean of three replicates ± SE (standard error). This means that a column followed by the same superscript ($P > 0.05$) differs according to Duncan's multiple range test., ***Significant at $P < 0.001$ level; ns-not significant. *** indicates $p < 0.001$ significcant.

(A) niger (8.45 ± 0.00), *K. pneumoniae* (8.15 ± 0.50), and *(B) subtilis* (7.55 ± 0.20). Meanwhile, plant extract was tested against the same microbial pathogen, and no inhibitory effect was observed at this concentration except *against E. coli* with an inhibition zone (6.50 ± 0.10 mm). The reason for that is the cell walls of gram-positive bacteria are composed of a negatively charged peptidoglycan that is substantially thicker than those of gram-negative bacteria, which makes gram-positive bacteria more resistant to the antibacterial therapy of plant extract. On the other hand, according to several studies, gram-negative bacteria have more susceptibility to antibacterial effect due to lipopolysaccharides (LPS) in their cell membranes that generate strong adhesion of plant extract onto their cell surface and exhibit antibacterial activity[55]. In conclusion, FC-Ag nanoparticles (NPs) that are stabilized by residual phytomolecules from *F. communis* exhibit enhanced antimicrobial activity against microbial pathogens. This improved effectiveness can be attributed to the small particle size, high surface area, and favorable surface-to-volume ratio of the NPs, which increase the interaction area with microorganisms and thereby enhance their antibacterial properties.

Additionally, the minimal inhibitory concentration of FC-AgNPs was evaluated as shown in Table 5. The results showed that FC-AgNPs have a significant antimicrobial activity with minimum (64.00 µg/mL) and maximum (˃512.00 µg/mL) MIC value (Fig. 13). The results reveal that the MIC of FC-AgNPs against *S. aureus* (64.00 µg/mL) followed by both *E. coli* and *C. albicans* (128.00 µg/mL), then *B. subtilis* and *K. pneumoniae* (256.00 µg/mL) and finally *P. aeruginosa* and *A. niger* with MIC (512.00 µg/mL). The exact mechanism behind the antimicrobial effects of AgNPs is still not fully understood. However, some studies suggest that AgNPs inhibit and kill bacteria primarily by releasing silver ions, which may contribute to the inactivation of nucleic acids within the cells. Additionally, the biological activity of AgNPs might be linked to the production of free radicals that easily attach to bacterial cell membranes, leading to accelerated cell death in pathogens. Furthermore, factors such as the concentration of AgNPs, as well as the type, size, and shape of the bacteria, play a significant role in determining the bactericidal mechanisms of AgNPs[56].

The therapeutic potential of biosynthesized nanoparticles extends beyond conventional antimicrobial applications into the realm of advanced cancer therapy and drug delivery systems[57]. Recent advances in nanotechnology have revolutionized cancer treatment by addressing critical challenges such as drug resistance, tumor heterogeneity, and systemic toxicity[58]. Smart nanoparticles, capable of responding to biological cues or environmental triggers, are emerging as transformative platforms for precise cancer treatment, offering enhanced permeability, retention characteristics, and targeted delivery to diseased tissues while minimizing damage to healthy cells[59]. The unique physicochemical properties of metallic nanoparticles, particularly silver nanoparticles, including their high surface-area-to-volume ratio, biocompatibility, and stability, position them as promising candidates for biomedical applications beyond their well-established antimicrobial efficacy.

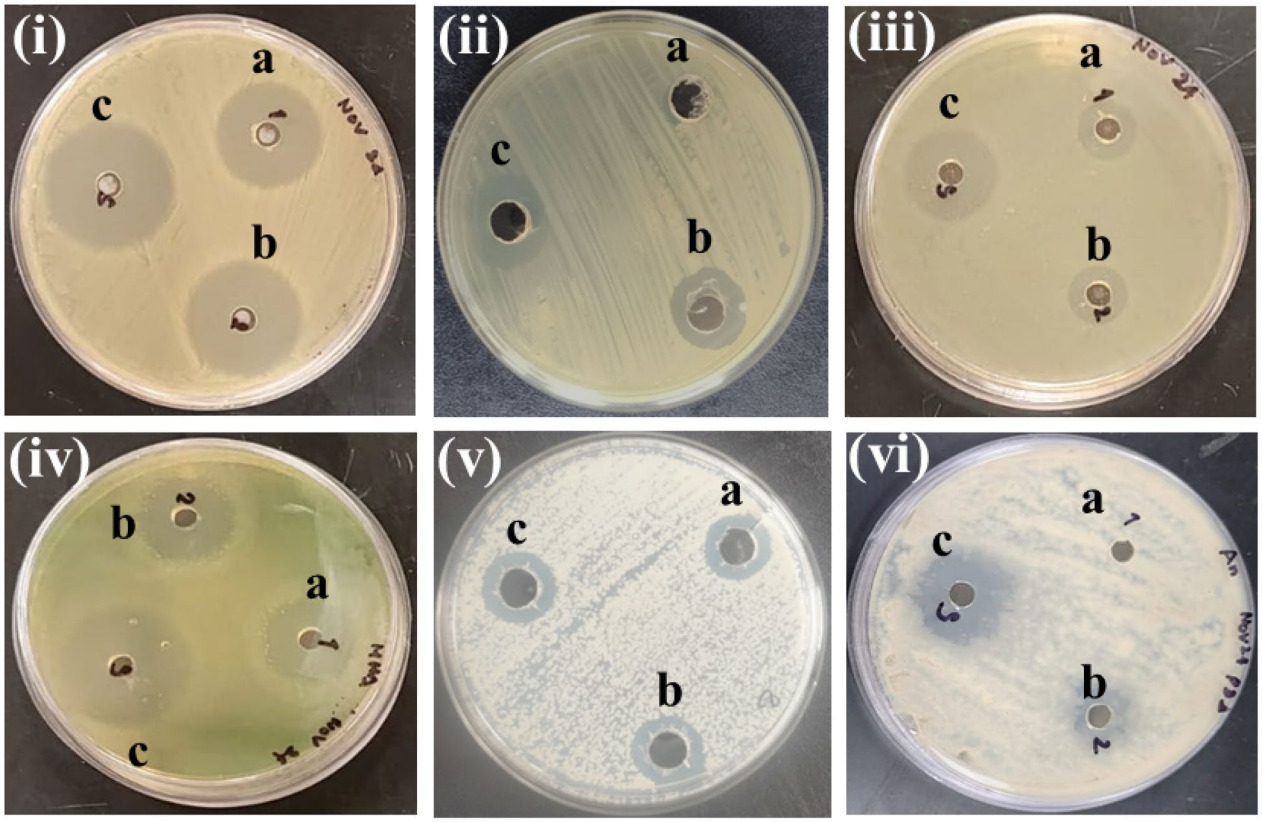

Fig. 11. Antibacterial activity of FCW and FC-AgNPs against microbial pathogens; (i) *S. aureus* ATCC12598, (ii) *B. subtilis* ATCC6051, (iii) *E. coli* ATCC25922, (iv) *P. aeruginosa* ATCC101450, (v) *C. albicans* ATCC2091, (vi) *A. niger* ATCC6275. (Note: Zones; a (FCW), b (FC-AgNPs) and c (std drugs; bacteria–Amoxicillin and fungi-Amphotericin B)).

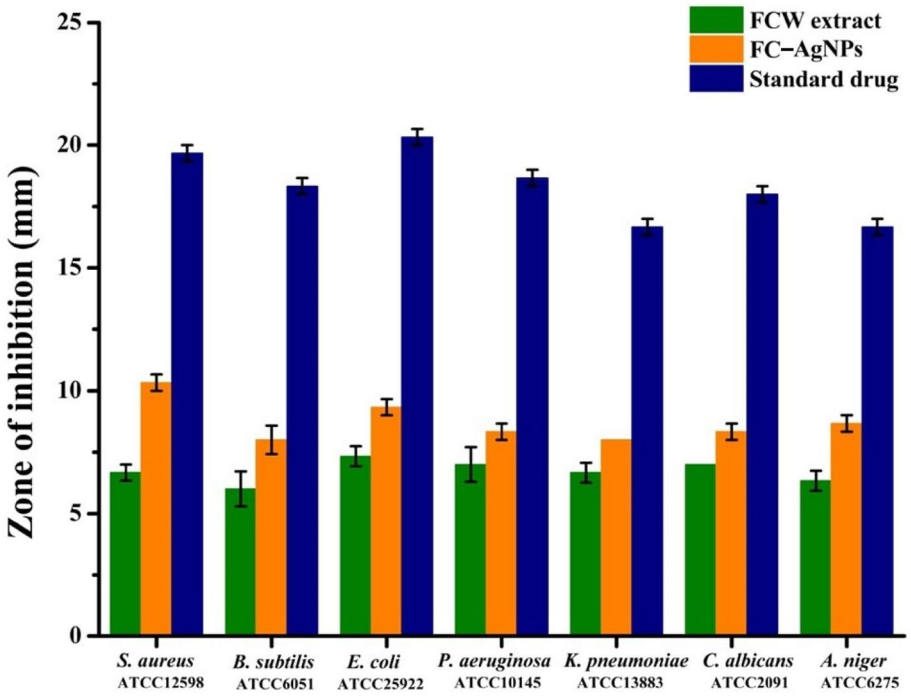

Fig. 12. Antimicrobial activity of water plant extract (FCW) and FC-AgNPs against microbial pathogens.

Microbial pathogens	MIC value (µg/mL)	
	FC-AgNPs	AMX
Gram positive bacteria		
S. aureus ATCC12598	64.00	≤10.00
B. subtilis ATCC6051	256.00	15.00
Gram negative bacteria		
E. coli ATCC25922	128.00	≤10.00
P. aeruginosa ATCC10145	>512.00	>10.00
K. pneumoniae ATCC13883	256.00	10.00
Fungi		**Amp B**
C. albicans ATCC2091	128.00	10.00
A. niger ATCC6275	512.00	15.00

Table 5. Determination of MIC of FC-AgNPs and standard drugs against microbial pathogens.

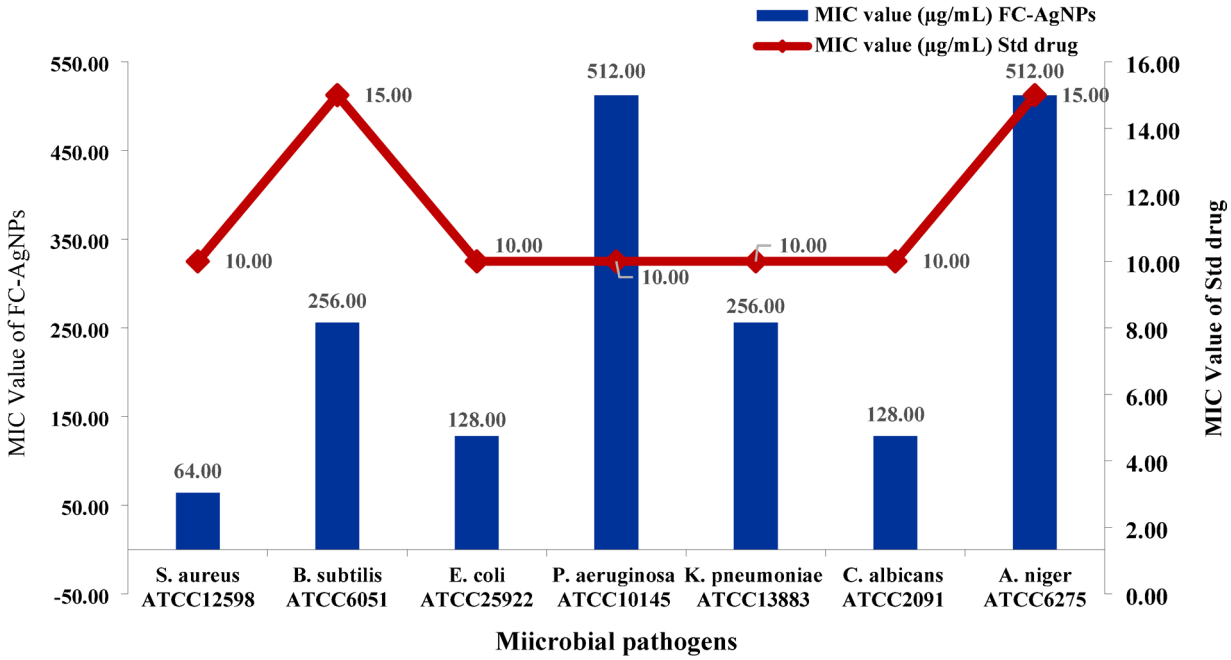

Fig. 13. MIC value of FC-AgNPs and standard drugs against microbial pathogens.

In the context of cancer therapeutics, nanoparticle-based drug delivery systems have demonstrated remarkable effectiveness in overcoming multidrug resistance through mechanisms such as efflux pump inhibition, targeted delivery to the tumor microenvironment, and enhanced cellular uptake. Notably, chloroquine, traditionally recognized as an antimalarial agent, has recently emerged as a potential anticancer agent for triple-negative breast cancer (TNBC) through autophagy inhibition, mitochondrial damage induction, and impairment of DNA repair mechanisms[60]. Studies on MDA-MB-231 cells have revealed that chloroquine significantly reduces cell viability, inhibits proliferation and migration, and demonstrates synergistic effects when combined with conventional chemotherapy, highlighting the importance of drug repurposing strategies in cancer treatment. The outstanding antimicrobial efficacy demonstrated by FC-AgNPs in this study—with minimum inhibitory concentrations (MICs) as low as 64.00 µg/mL against *Staphylococcus aureus* and 128.00 µg/mL against *Escherichia coli* and *Candida albicans*—strongly suggests their potential application as anticancer agents. The synergistic interaction between silver ions released from the nanoparticle surface and the phytoconstituents (particularly stigmasterol, pentadecanoic acid, and ferutinin derivatives) embedded within the nanoparticles creates a multifaceted therapeutic platform. These compounds possess documented anticancer and antiproliferative properties that, when combined with the silver nanoparticles inherent capacity to generate reactive oxygen species (ROS) and cause cellular membrane disruption, present substantial promise for inhibiting cancer cell proliferation and inducing apoptosis through mechanisms similar to those observed with chloroquine.

The antibacterial efficacy of biosynthesized silver nanoparticles observed in this study aligns with recent findings demonstrating the potent antimicrobial properties of AgNPs against diverse bacterial pathogens[46]. Riazunnisa (2023) reported that silver nanoparticles synthesized using *Bauhinia racemosa* leaf extracts exhibited

significant antibacterial activity against both Gram-positive (*S. aureus*) and Gram-negative bacteria (*E. coli*, *K. pneumoniae*, *P. aeruginosa*), with characteristic surface plasmon resonance bands at 430 nm for aqueous extracts and 360 nm for methanolic extracts, confirming successful nanoparticle formation[61]. The antibacterial mechanism involves multiple synergistic pathways, including bacterial membrane disruption, generation of reactive oxygen species (ROS), and interference with DNA replication processes. The size-dependent antibacterial activity is particularly noteworthy, as smaller nanoparticles exhibit enhanced membrane penetration capabilities and greater bactericidal effects. Studies have demonstrated that AgNPs function through direct interaction with bacterial cell walls, altering membrane permeability and ultimately causing cellular disruption[62]. The electrostatic interaction between positively charged silver ions released from AgNPs and negatively charged bacterial cell walls facilitates enhanced antimicrobial activity. Furthermore, the concentration-dependent antibacterial behavior observed in various studies indicates that AgNPs exhibit bacteriostatic properties at lower concentrations and bactericidal effects at higher concentrations, with minimum inhibitory concentrations (MICs) typically ranging from 3.9 to 100 µg/mL depending on bacterial species and nanoparticle characteristics[63]. These mechanisms collectively explain the superior antimicrobial performance of plant-mediated silver nanoparticles against multidrug-resistant bacterial strains.

The antimicrobial performance of FC-AgNPs synthesized in this study demonstrates competitive to moderately enhanced activity when compared with similar plant-mediated silver nanoparticle systems reported in recent literatures. The FC-AgNPs exhibited inhibition zones ranging from 7.55 mm (*B. subtilis*) to 10.05 mm (*S. aureus*) with MIC values between 64 µg/mL (*S. aureus*) and 512 µg/mL (*P. aeruginosa* and *A. niger*). This antimicrobial efficacy positions FC-AgNPs within the moderate-to-strong activity range when benchmarked against comparable biosynthesized systems[64–66]. Silver nanoparticles synthesized using *Bauhinia racemosa* exhibited similar inhibition zones against *S. aureus* and *E. coli*, while AgNPs from *Carduus crispus* showed inhibition zones of 6.5–7.7 mm—comparable to the lower range of FC-AgNPs activity[61,67]. AgNPs synthesized from *Gnidia lanceolarium* reported MIC values of 43.94 µg/mL against *S. aureus*, which is slightly better than FC-AgNPs (64 µg/mL). Plant-based AgNPs from *Eucalyptus camaldulensis* and *Terminalia arjuna* showed inhibition zones of 16–17 mm—higher than FC-AgNPs, suggesting that specific phytochemical compositions and synthesis optimization significantly influence antimicrobial efficacy[68]. Notably, FC-AgNPs do not achieve the exceptionally low MIC values observed in optimized bacterial or chemically-enhanced systems, they demonstrate solid moderate-level antimicrobial activity comparable to many plant-mediated systems and offer the distinct advantage of being derived from a medicinally valuable plant with a rich phytochemical profile that potentially extends their applications beyond simple antimicrobial use.

The identification of 67 distinct bioactive compounds through GC-MS provides strong mechanistic insight into the reducing and stabilizing roles of specific phytochemicals, particularly stigmasterol (18.2%), pentadecanoic acid (7.6%), and ferutinin derivatives. The study demonstrates superior antimicrobial efficacy compared to the crude plant extract alone, confirming genuine nanoparticle contribution to biological activity. Additionally, the use of an eco-friendly, cost-effective green synthesis methodology represents a sustainable alternative to conventional chemical synthesis, with clear optimization of reaction parameters (temperature, time, extract concentration) enhancing reproducibility and yield. The antimicrobial activity, while significant, falls within the moderate range when compared to highly optimized nanoparticle systems, with MIC values (64–512 µg/mL) higher than some chemically-synthesized alternatives. However, additional microbial strains still need to be evaluated to establish broader generalizability for the claimed broad-spectrum activity. Moreover, further mechanistic studies—such as molecular docking, genomic profiling, or advanced imaging—are required to elucidate the precise antimicrobial mechanisms, beyond the currently understood general pathways reported for AgNPs. Nevertheless, the integration of green synthesis methodologies with advanced functionalization strategies could potentially expand the biomedical applications of plant-mediated nanoparticles from antimicrobial agents to multifunctional therapeutic platforms for targeted cancer therapy and personalized medicine.

Conclusions

This study successfully demonstrated the green synthesis of FC-AgNPs using an aqueous extract of *F. communis*. The method presented is sustainable, cost-effective, and environmentally friendly. The biosynthesis process was optimized by adjusting the concentration of the plant extract, reaction time, and temperature. Characterization techniques confirmed the formation of predominantly spherical, crystalline AgNPs with an average diameter of ~ 26.6 nm. FTIR analysis indicated that phenolics, terpenoids, and sterols played a role in both the reduction and stabilization of AgNPs. Additionally, GC-MS analysis identified 67 phytochemicals in the extract, with stigmasterol, pentadecanoic acid, (5*E*, 9*Z*)-farnesyl acetone, and pentyl docosanoate being among the most significant contributors to the synthesis process. The biosynthesized FC-AgNPs demonstrated significant antimicrobial activity against a wide range of microbial strains, surpassing the effectiveness of the crude plant extract. This enhanced activity is likely due to the combined effects of silver ions and the phytoconstituents that cap the surface of the NPs, which together contribute to disrupting microbial membranes and causing cell death. Notably, *S. aureus* and *E. coli* showed the highest susceptibility to the NPs, exhibiting inhibition zones of 10.05 ± 0.05 mm and 9.25 ± 0.05 mm, respectively. The study also identified minimum inhibitory concentrations (MICs) as low as 64 µg/mL for certain pathogens, highlighting the therapeutic potential of FC-AgNPs. Thus, the green synthesis of AgNPs using *F. communis* extract presents a promising alternative to traditional methods, with important implications for biomedical and pharmaceutical applications, particularly in antimicrobial therapies.

Data availability

Data contained within the Article.

Received: 30 August 2025; Accepted: 18 December 2025
Published online: 27 December 2025

References

1. Verma, A., Gautam, S. P., Bansal, K. K., Prabhakar, N. & Rosenholm, J. M. Green nanotechnology: advancement in phytoformulation research. *Medicines* **6**, 39 (2019).
2. Khan, F. et al. Green nanotechnology: Plant-Mediated nanoparticle synthesis and application. *Nanomaterials* **12**, 673 (2022).
3. Jain, P. K., Huang, X., El-Sayed, I. H. & El-Sayed, M. A. Review of some interesting surface plasmon resonance-enhanced properties of noble metal nanoparticles and their applications to biosystems. *Plasmonics* **2**, 107–118 (2007).
4. Abdelghany, T. M. et al. Recent advances in green synthesis of silver nanoparticles and their applications: about future directions. *Rev. Bionanoscience*. **8**, 5–16 (2018).
5. Tripathi, N. & Goshisht, M. K. Recent advances and mechanistic insights into antibacterial Activity, antibiofilm Activity, and cytotoxicity of silver nanoparticles. *ACS Appl. Bio Mater.* **5**, 1391–1463 (2022).
6. Durán, N. et al. Silver nanoparticles: A new view on mechanistic aspects on antimicrobial activity. *Nanomedicine* **12**, 789–799 (2016).
7. Feng, Q. L. et al. A mechanistic study of the antibacterial effect of silver ions on Escherichia coli and Staphylococcus aureus. *J. Biomed. Mater. Res.* **52**, 662–668 (2000).
8. Slepička, P., Slepičková Kasálková, N., Siegel, J., Kolská, Z. & Švorčík, V. Methods of gold and silver nanoparticles Preparation. *Mater. (Basel)*. **13**, 1 (2019).
9. Abou El-Nour, K. M. M., Eftaiha, A., Al-Warthan, A. & Ammar, R. A. A. Synthesis and applications of silver nanoparticles. *Arab. J. Chem.* **3**, 135–140 (2010).
10. Sharma, N. K. et al. Green route synthesis and characterization techniques of silver nanoparticles and their biological adeptness. *ACS Omega*. **7**, 27004–27020 (2022).
11. Rizwana, H. et al. Green biosynthesis of silver nanoparticles using vaccinium oxycoccos (Cranberry) extract and evaluation of their biomedical potential. *Cryst. (Basel)*. **13**, 294 (2023).
12. Ahmad, S. et al. Green nanotechnology: a review on green synthesis of silver nanoparticles - an ecofriendly approach. *Int. J. Nanomed.* **14**, 5087–5107 (2019).
13. Vidyasagar, N., Patel, R. R., Singh, S. K. & Singh, M. Green synthesis of silver nanoparticles: methods, biological applications, delivery and toxicity. *Mater. Adv.* **4**, 1831–1849 (2023).
14. Gardea-Torresdey, J. L. et al. Formation and Growth of Au Nanoparticles inside Live Alfalfa Plants. *Nano Letters* **2**, 397–401 (2002).
15. Nadagouda, M. N. & Varma, R. S. Green synthesis of silver and palladium nanoparticles at room temperature using coffee and tea extract. *Green Chem.* **10**, 859–886 (2008).
16. Ajlouni, A. W. et al. Green synthesis of silver nanoparticles using aerial part extract of the anthemis Pseudocotula Boiss. Plant and their biological activity. *Molecules* **28**, 246 (2022).
17. Neghliz, H. & Benabdelkader, T. Antimicrobial and antioxidant activities of the essential oils from different organs of ferula communis L. growing wild in Algeria. African Review of Science, Technology and Development **6**, 1–9 (2021).
18. Deniz, G. Y., Laloglu, E., Koc, K. & Geyikoglu, F. Hepatoprotective potential of ferula communis extract for carbon tetrachloride induced hepatotoxicity and oxidative damage in rats. *Biotech. Histochem.* **94**, 334–340 (2019).
19. Akaberi, M., Iranshahy, M. & Iranshahi, M. Review of the traditional uses, phytochemistry, Pharmacology and toxicology of giant fennel (Ferula communis L. subsp. communis). *Iran. J. Basic. Med. Sci.* **18**, 1050–1062 (2015).
20. Monti, M. et al. Characterization of anti-coagulant properties of prenylated coumarin ferulenol. *Biochim. Biophys. Acta*. **1770**, 1437–1440 (2007).
21. Ed-Dahmani, I. et al. Ferula communis leaf extract: antioxidant capacity, UHPLC–MS/MS analysis, and in vivo and in Silico toxicity investigations. *Front. Chem.* **12**, 1485463 (2025).
22. Bocca, C., Gabriel, L., Bozzo, F. & Miglietta, A. Microtubule-interacting activity and cytotoxicity of the prenylated coumarin ferulenol. *Planta Med.* **68**, 1135–1137 (2002).
23. Appendino, G. et al. Antimycobacterial coumarins from the Sardinian giant fennel (Ferula communis). *J. Nat. Prod.* **67**, 2108–2110 (2004).
24. Yirdaw, B. & Kassa, T. Preliminary phytochemical screening and antibacterial effects of root bark of ferula communis (Apiaceae). *Vet. Med. Sci.* **9**, 1901–1907 (2023).
25. Rahali, F. Z. et al. Biochemical characterization of fennel (Ferula communis l.) different parts through their essential oils, fatty acids and phenolics. *Acta Scientiarum Polonorum Hortorum Cultus*. **20**, 3–14 (2021).
26. Pandey, K. B. & Rizvi, S. I. Plant polyphenols as dietary antioxidants in human health and disease. *Oxid. Med. Cell. Longev.* **2**, 270–278 (2009).
27. Maiuolo, J. et al. The effect of ferula communis extract in Escherichia coli lipopolysaccharide-induced neuroinflammation in cultured neurons and oligodendrocytes. *Int. J. Mol. Sci.* **22**, 7910 (2021).
28. Al-Yahya, M. A., Muhammad, I., Mirza, H. H. & El-Feraly, F. S. Antibacterial constituents from the rhizomes of ferula communis. *Ltd. Phytother Res.* **12**, 335–339 (1998).
29. Khan, M. et al. Green synthesis of silver nanoparticles using Juniperus procera extract: their Characterization, and biological activity. *Cryst. (Basel)*. **12**, 420 (2022).
30. MubarakAli, D., Thajuddin, N., Jeganathan, K. & Gunasekaran, M. Plant extract mediated synthesis of silver and gold nanoparticles and its antibacterial activity against clinically isolated pathogens. *Colloids Surf. B Biointerfaces*. **85**, 360–365 (2011).
31. Barry, A., Bryskier, A., Traczewski, M. & Brown, S. Preparation of stock solutions of macrolide and ketolide compounds for antimicrobial susceptibility tests. *Clin. Microbiol. Infect.* **10**, 78–83 (2004).
32. Khan, M., Mahmood, A. & Alkhathlan, H. Z. Characterization of leaves and flowers volatile constituents of Lantana Camara growing in central region of Saudi Arabia. *Arab. J. Chem.* **9**, 764–774 (2016).
33. Linstrom, P. & Chemistry WebBook, M. W. N. I. S. T. NIST Standard Reference Database Number 69, June 2005. National Institute of Standards and Technology, Gaithersburg MD 20899, (n.d.). (2025). https://webbook.nist.gov/chemistry/
34. Acree, T. A. H. Gas chromatography-olfactometry (GCO) of natural products. Flavornet and human odor space, Sponsored by DATU Inc. (2004). https://www.flavornet.org/
35. Babushok, V. I., Linstrom, P. J. & Zenkevich, I. G. Retention indices for frequently reported compounds of plant essential oils. *J Phys. Chem. Ref. Data* **40**, 043101 (2011).
36. Adams, R. P. *Identification of Essential Oil Components by Gas Chromatography/Mass Spectrometry* (Allured Business Media, 2017).
37. Mohammadi, F., Yousefi, M. & Ghahremanzadeh, R. Green Synthesis, characterization and antimicrobial activity of silver nanoparticles (AgNps) using leaves and stems extract of some plants. *Adv. J. Chem. Sect. A*. **2**, 266–275 (2019).
38. Javed, M. A. et al. Biosynthesis and characterization of silver nanoparticles from cedrela Toona leaf extracts: an exploration into their antibacterial, anticancer, and antioxidant potential. *Green. Process. Synthesis*. **13**, 20230248 (2024).
39. Khairunnisa, S., Wonoputri, V. & Samadhi, T. W. Effective deagglomeration in biosynthesized nanoparticles: A mini review. *IOP Conf. Ser. Mater. Sci. Eng.* **1143**, 012006 (2021).
40. Zuas, O., Hamim, N. & Sampora, Y. Bio-synthesis of silver nanoparticles using water extract of myrmecodia Pendan (Sarang Semut plant). *Mater. Lett.* **123**, 156–159 (2014).

41. Hosseinpour-Mashkani, S. M. & Ramezani, M. Silver and silver oxide nanoparticles: synthesis and characterization by thermal decomposition. *Mater. Lett.* **130**, 259–262 (2014).
42. Pham, Q. T., Huy, B. T. & Lee, Y. I. New highly efficient electrochemical synthesis of dispersed Ag2O particles in the vicinity of the cathode with controllable size and shape. *J. Mater. Chem. C Mater.* **3**, 7720–7726 (2015).
43. Afshinnia, K., Marrone, B. & Baalousha, M. Potential impact of natural organic ligands on the colloidal stability of silver nanoparticles. *Sci. Total Environ.* **625**, 1518–1526 (2018).
44. Wongsa, P., Phatikulrungsun, P. & Prathumthong, S. FT-IR characteristics, phenolic profiles and inhibitory potential against digestive enzymes of 25 herbal infusions. *Sci. Rep.* **12**, 6631 (2022).
45. Saeidy, S. et al. Structural characterization and thermal behavior of a gum extracted from ferula Assa foetida L. *Carbohydr. Polym.* **181**, 426–432 (2018).
46. Kiranmayee, M. & Riazunnisa, K. Bioactive phytochemical compounds characterization, anti-oxidant and anti-microbial activity of the methanol and acetonitrile leaf extracts of pithecellobium Dulce. *Phytomedicine Plus.* **5**, 100760 (2025).
47. Marslin, G. et al. Secondary metabolites in the green synthesis of metallic nanoparticles. *Mater. (Basel).* **11**, 940 (2018).
48. Antunes Filho, S. et al. Biosynthesis of nanoparticles using plant extracts and essential oils. *Molecules* **28**, 3060 (2023).
49. Bouttier-Figueroa, D. C., Cortez-Valadez, J. M., Flores-Acosta, M. & Robles-Zepeda, R. E. Synthesis of metallic nanoparticles using plant's natural extracts: synthesis mechanisms and applications. *Biotecnia* **25**, 125–139 (2023).
50. Al-Sheddi, E. S. et al. Anticancer potential of green synthesized silver nanoparticles using extract of nepeta deflersiana against human cervical cancer cells (HeLA). *Bioinorg Chem Appl.* **2018**, 9390784. (2018).
51. Mondal, M. S., Paul, A. & Rhaman, M. Recycling of silver nanoparticles from electronic waste via green synthesis and application of AgNPs-chitosan based nanocomposite on textile material. *Sci. Rep.* **13**, 13798 (2023).
52. Ismail, M., Gul, S., Khan, M. A. & Khan, M. I. Plant mediated green synthesis of Anti-Microbial silver Nanoparticles—A review on recent trends. *Reviews Nanosci. Nanatechnol.* **5**, 119–135 (2018).
53. Almatroudi, A. Silver nanoparticles: Synthesis, characterisation and biomedical applications. *Open. Life Sci.* **15**, 819–839 (2020).
54. Mehrotra, S., Goyal, V., Dimkpa, C. O. & Chhokar, V. Green synthesis and characterization of Ginger-Derived silver nanoparticles and evaluation of their Antioxidant, Antibacterial, and anticancer activities. *Plants* **13**, 1255 (2024).
55. Jaffar, S. S. et al. Green synthesis of Flower-Like Carrageenan-Silver nanoparticles and Elucidation of its physicochemical and antibacterial properties. *Molecules* **28**, 907 (2023).
56. Loo, Y. Y. et al. In vitro antimicrobial activity of green synthesized silver nanoparticles against selected Gram-negative foodborne pathogens. *Front. Microbiol.* **9**, 1555 (2018).
57. Kirubakaran, D. Herbal remedies for alzheimer's disease: neuroprotective mechanisms and cognitive enhancement potential. *Digit. Chin. Med.* **8**, 183–195 (2025).
58. Kirubakaran, D. Review on emerging frontiers in medical sensing: innovations shaping the future of healthcare. *Biomedical Mater. Devices.* **1–21** https://doi.org/10.1007/s44174-025-00385-3 (2025).
59. Kirubakaran, D. & Krishnan, V. Toxicological profile and therapeutic potentials of impatiens chinensis leaf extract: exploring antibacterial, antioxidant, antidiabetic and insecticidal properties. *Pharmacol. Res. - Nat. Prod.* **7**, 100238 (2025).
60. Dayalan, H., Bupesh, G., Kirubakaran, D., Mathe, D. & Panigrahi, J. Chloroquine as a potential anticancer agent for triple-negative breast cancer: effects on MDA-MB-231 cells. *Med. Oncol.* **42**, 245 (2025).
61. Riazunnisa, K. Antimicrobial activity of biosynthesized silver nanoparticles of bauhinia racemosa leaf extracts. *Res. J. Pharm. Technol.* **16**, 745–749 (2023).
62. Yousef, H. A., Salah, M. A., Riazunnisa, K. & Habeeb, K. Noble silver nanoparticles (AgNPs) synthesis and characterization of Fig ficus carica (fig) leaf extract and its antimicrobial effect against clinical isolates from corneal ulcer. *Afr. J. Biotechnol.* **13**, 4275–4281 (2014).
63. Khateef, R. et al. Potential in-vitro anti-breast cancer activity of green-synthesized silver nanoparticles Preparation against human MCF-7 cell-lines. *Adv. Nat. Sci. NanoSci. NanoTechnol.* **10**, 045012 (2019).
64. Wahab, S., Khan, T., Adil, M. & Khan, A. Mechanistic aspects of plant-based silver nanoparticles against multi-drug resistant bacteria. *Heliyon* **7**, e07448 (2021).
65. Ramírez Aguirre, D. P. et al. Comparative antibacterial potential of silver nanoparticles prepared via chemical and biological synthesis. *Arab. J. Chem.* **13**, 8662–8670 (2020).
66. Mohanta, Y. K. et al. Anti-biofilm and antibacterial activities of silver nanoparticles synthesized by the reducing activity of phytoconstituents present in the Indian medicinal plants. *Front. Microbiol.* **11**, 1143 (2020).
67. Urnukhsaikhan, E., Bold, B. E., Gunbileg, A., Sukhbaatar, N. & Mishig-Ochir, T. Antibacterial activity and characteristics of silver nanoparticles biosynthesized from carduus Crispus. *Sci. Rep.* **11**, 21047 (2021).
68. Liaqat, N., Jahan, N., Khalil-ur-Rahman, Anwar, T. & Qureshi, H. Green synthesized silver nanoparticles: Optimization, characterization, antimicrobial activity, and cytotoxicity study by hemolysis assay. *Front. Chem.* **10**, 952006 (2022).

Acknowledgements

The authors would like to acknowledge the funding from the Ongoing Research Funding Program (ORF-2025-817), King Saud University, Riyadh, Saudi Arabia.

Author contributions

Conceptualization, H.Z.A. and Me.K.; methodology, Y.M.G.A., Me.K. and H.Z.A.; software, P.K. and Me.K.; validation, E.Y.D. and A.A.; formal analysis, P.K., A.A. and M.R.S.; investigation, Y.M.G.A. and Me.K.; resources, Me.K. and H.Z.A.; data curation, Muj.K., S.F.A. and M.R.S.; writing—original draft preparation, Y.M.G.A.; writing—review and editing, Muj.K., S.F.A., M.R.S. and Me.K.; performed the formal analysis of the plant extract material, Y.M.G.A. and Me.K.; visualization, E.Y.D.; supervision, H.Z.A., E.Y.D. and Me.K.; project administration, H.Z.A. and Me.K.; funding acquisition, H.Z.A.

Funding

The authors would like to acknowledge the funding from the Ongoing Research Funding Program (ORF-2025-817), King Saud University, Riyadh, Saudi Arabia.

Declarations

Competing interests

The authors declare no competing interests.

Additional information

Correspondence and requests for materials should be addressed to H.Z.A. or M.K.